Development of early postnatal inhibitory function in the mouse medial prefrontal and primary somatosensory cortex

Katerina Kalemaki[1,2], Xiaxia Xu[3], Angeliki Velli[2,4], Ourania Christodoulou[4,5], Myrto Denaxa[5] Ileana L. Hanganu-Opatz[3], Domna Karagogeos[1, 2*] and Kyriaki Sidiropoulou[2,4*]

[1]Department of Basic Science, Faculty of Medicine, University of Crete, Heraklion, Greece

[2]Institute of Molecular Biology and Biotechnology (IMBB), FORTH, Heraklion, Greece

[3]Developmental Neurophysiology, Institute of Neuroanatomy, University Medical Center Hamburg-Eppendorf, Hamburg, Germany

[4]Department of Biology, University of Crete, Heraklion, Greece

[5]BSRC 'Alexander Fleming'

[*] co-corresponding author and equal senior contribution

Abstract

The prefrontal cortex (PFC) is characterized by protracted maturation that extends until adulthood. The cellular mechanisms controlling the early development of prefrontal circuits are still largely unknown. Our study delineates the developmental cellular processes that are on-going in the mouse medial PFC (mPFC) during the second and third postnatal weeks and compares them to those in the barrel cortex (BC). We show that basal synaptic transmission decreases from the second to the third postnatal week in both brain areas due to increased spontaneous inhibitory currents and reduced excitatory ones. Moreover, the GABAergic interneurons in the neonatal mPFC exhibit immature active properties. Furthermore, increasing $GABA_A$ receptor ($GABA_AR$) activity leads to increased basal synaptic response and spontaneous activity of neonatal mPFC, but not BC. Additionally, the K-Cl co-transporter 2 (KCC2) expression is decreased in the neonatal mPFC compared to the pre-juvenile one as well as to the neonatal and pre-juvenile BC, suggesting that $GABA_AR$ function in the neonatal mPFC is depolarizing. Therefore, our study reveals two significant differences in the maturation of GABAergic function of mPFC compared to BC: a developmental delay in the depolarizing function of GABA and the immature active properties of GABAergic interneurons.

32

33 **Abbreviations**

34 BC: Barrel Cortex

35 mPFC: medial Prefrontal Cortex

36 P10: Postnatal day 10

37 PNs: Pyramidal neurons

38 INs: Interneurons

39

40 **Introduction**

41 During early postnatal development, major events that contribute to cortical circuit
42 maturation include spatial and temporal patterns of electrical activity, intrinsically determined
43 cell death of early postnatal cortical interneurons and the depolarizing action of the
44 neurotransmitter GABA (γ-aminobutyric acid) (Khazipov et al. 2004; Khazipov and Luhmann
45 2006; Allene et al. 2008; Brockmann et al. 2011; Ben-Ari et al. 2012; Southwell et al. 2012;
46 Khazipov et al. 2013; Kirmse et al. 2015; Mòdol et al. 2019). The developmental switch of GABA
47 action from depolarizing to hyperpolarizing results from changes in chloride co-transporter
48 expression: Na^+-K^+-Cl^- cotransporter 1 (NKCC1), the Cl^- importer, is highly expressed early in
49 development, while the expression of the co-transporter KCC2, the Cl^- exporter, increases after
50 the first postnatal week (Ben-Ari 2001; 2002; Ben-Ari et al. 2007; Ben-Ari 2012). In addition, both
51 intrinsic properties of neurons and synaptic transmission undergo dramatic changes during early
52 postnatal development in a brain-area specific manner (Kriegstein et al. 1987; McCormick and
53 Prince 1987; Burgard and Hablitz 1993; Ramoa and McCormick 1994; Bahrey and Moody 2003).
54 Most studies on these developmental changes of the GABAergic system in the cortex have
55 focused on the primary somatosensory cortex, visual cortex and hippocampus (Bartolini et al.
56 2013; Le Magueresse and Monyer 2013; Hensch 2016). The barrel cortex (BC) is part of the
57 primary somatosensory cortex and is organized vertically in columns of cells associated with
58 sensory perception (Guo et al. 2014) and horizontally in six layers of distinct cell types. In
59 contrast, cortical association areas such as the prefrontal cortex (PFC) regulate cognitive
60 functions and do not directly control sensory information (Fuster 2015). Anatomically, the
61 mouse medial PFC (mPFC) is defined as the agranular part of frontal lobe, lacking the prominent
62 granular layer IV and is divided into distinct subregions, namely infralimbic, prelimbic and
63 cingulate cortex (Heidbreder and Groenewegen 2003; Van De Werd et al. 2010). The timeline of

mPFC development is delayed compared to other sensory cortices, such as BC (Casey et al. 2000; Best and Miller 2010; Kolb et al. 2012). From infancy to adulthood, the developing mPFC undergoes considerable transcriptional, structural and functional changes (Diamond 2005; Tsujimoto 2008; Kolb et al. 2012; Schubert et al. 2014; Kroeze et al. 2017).

While adolescent development of prefrontal circuitry and the underlying cellular mechanisms have been addressed by a large number of studies, only few investigations tackled the wiring processes at earlier stages (Brockmann et al. 2011; Bitzenhofer et al. 2015; 2017). However, specific knowledge is missing for the physiological and cellular changes that are on-going in the mPFC between the second (neonatal) and third (pre-juvenile) postnatal week. Here, we aim to fill this gap by investigating the synaptic and intrinsic properties of neonatal and pre-juvenile mPFC neurons and comparing them to those in the BC, with a primary focus on the GABAergic system.

Methods

All *in vitro* experiments with mice took place under an experimental protocol approved by the Research Ethics Committee and by our Institutional Animal Care and Use Committee that has been approved by the Veterinarian Authorities Office (protocol license no. 93164). Experiments were carried out by trained scientists and in accordance with the 3R principles. *In vivo* experiments were performed in compliance with the German laws and the guidelines of the European Community for the use of animals in research and were approved by the local ethical committee (015/17, 015/18).

Animals

The *in vitro* experiments were performed on male C57Bl/6J; Lhx6Tg(Cre); R26R-YFP+/+ mice from animal facility of IMBB-FORTH were used. For the *in vivo* experiments, timed-pregnant C57BL/6J mice from the animal facility of the University Medical Center Hamburg-Eppendorf were used. The day of vaginal plug detection was defined as embryonic day (E)0.5, whereas the day of birth was defined as P0. The offspring of both sexes are used for *in vivo* electrophysiology recordings. All procedures were performed according to the European Union ethical standards outlined in the Council Directive 2010/63EU of the European Parliament on the protection of animals used for scientific purposes.

95 Mice were housed with their mothers and provided with standard mouse chow and water ad
96 libitum, under a 12 h light/dark cycle (light on at 7:00 am) with controlled temperature (21°C).
97 The P10 experimental group includes ages P9-P11 and the P20 group includes ages P19-P21, also
98 referred to as second and third postnatal weeks or neonatal and pre-juvenile, respectively. All
99 efforts were made to minimize both the suffering and the number of animals used.
100

101 ***In vitro* extracellular recordings**

102 Slice Preparation*:* Mice (P10 and P20) were decapitated under halothane anesthesia. The brain
103 was removed promptly and placed in ice cold, oxygenated (95% O_2 –5% CO_2) artificial
104 cerebrospinal fluid (aCSF) containing (in mM): 125 NaCl, 3.5 KCl, 26 $NaHCO_3$, 1 $MgCl_2$ and 10
105 glucose (pH = 7.4, 315 mOsm/l). The brain was blocked and glued onto the stage of a vibratome
106 (Leica, VT1000S). Rostrocaudal coronal slices (400 µm thick) containing either the mPFC
107 (prefrontal cortex) or the BC (barrel cortex) region were selected and transferred to a submerged
108 chamber, which was continuously superfused with oxygenated (95% O_2 –5% CO_2) aCSF
109 containing (in mM): 125 NaCl, 3.5 KCl, 26 $NaHCO_3$, 2 $CaCl_2$, 1 $MgCl_2$ and 10 glucose (pH = 7.4, 315
110 mOsm/l) at room temperature (RT). The slices were allowed to equilibrate for at least 1 h in this
111 chamber before recordings began. Slices were then transferred to a submerged recording
112 chamber, continuously superfused with oxygenated (95% O_2 –5% CO_2) aCSF (same constitution
113 as the one used for maintenance of brain slices) at RT during recordings.

114 Data Acquisition: Electrophysiological recordings were performed in all experimental groups
115 under the same conditions as described below. Pulled glass micropipettes were filled with NaCl
116 (2M) and placed in layers II/III of PFC and BC. Platinum/iridium metal microelectrodes (Harvard
117 apparatus United Kingdom, 161 Cambridge, United Kingdom) were placed on layer II/III of the
118 mPFC and the BC, about 300 µm away from the 1MΩ recording electrode, and were used to
119 evoke field excitatory postsynaptic potentials (fEPSPs). Local field potentials (LFPs) were
120 amplified using a headstage with selectable high pass filter of 30 Hz to remove any offsets
121 coupled to a Dagan BVC-700A amplifier, amplified 100 times and low-pass filtered at 1-kHz. A
122 notch filter was used to eliminate line frequency noise at 30 Hz. Signals were digitized using the
123 ITC-18 board (InstruTech, Inc.) on a PC with custom-made procedures in IgorPro (Wavemetrics,
124 Inc.) and stored on a PC hard drive. All voltage signals were collected at a sampling frequency of
125 100 kHz (fs = 100 kHz).

126 For evoked fEPSPs, the electrical stimulus consisted of a single square waveform of 100 μs
127 duration given at intensities of 0.1– 0.3 mA (current was increased from 0.1 mA to 0.3 mA, with
128 0.1 mA steps) generated by a stimulator equipped with a stimulus isolation unit (World Precision
129 Instruments, Inc.). The effect of $GABA_AR$ activation was investigated by bath application of 2 μM
130 Diazepam ($GABA_AR$ agonist). Diazepam was acquired from the Pharmacy of the University
131 General Hospital in Heraklion as a 5 mg/ml solution and was diluted in aCSF during recordings.
132 Other drugs used include CNQX (10μM), AP5 (50μM) and bumetanide (10μM) (Tocris). For
133 spontaneous activity recordings, 20 5-sec recordings were acquired without any stimulation.
134 Data Analysis: Data were analyzed using custom-written procedures in IgorPro software
135 (Wavemetrics, Inc.). No additional high-pass filters were applied to the raw data. For evoked
136 recordings, the peak values of the fEPSP were measured using the minimum value of the synaptic
137 response (4–5 ms following stimulation) and were compared to the baseline value prior to
138 stimulation. Both parameters were monitored in real- time in every experiment. A stimulus–
139 response curve was then plotted using stimulation intensities between 0.1 and 0.8 mA, in 0.1
140 mA steps. For each different intensity level, two traces were acquired and averaged.
141 To identify spontaneous activity events, the acquired spontaneous activity voltage signals of 5
142 seconds' duration were decimated (down-sampled) by a factor of 10 and the standard deviation
143 σ_b of background signal was calculated in the 'quiet' part of each voltage response trace. To
144 identify the 'quiet' period, each 5sec trace was split into 100msec increments and the range of
145 voltage deflection was computed in each increment. The 'quiet' part of the LFP trace was the
146 100msec increment with the smallest σ_b value. As a spontaneous event, any voltage response
147 larger than $4 \cdot \sigma_b$ was identified. We calculated the frequency of spontaneous events by
148 measuring the number of spontaneous events divided by the duration of the trace (5s). The
149 frequency was calculated in 20 consecutive 5-sec traces and then averaged for each condition
150 animal. The spontaneous events do not correspond to spiking of individual neurons, they rather
151 reflect population spikes.
152
153 ***In vitro* patch-clamp recordings**
154 Slice Preparation: Mice were decapitated under halothane anesthesia. The brain was removed
155 immediately and coronal slices of mPFC and BC (300–350 μm thick), using a vibratome (Leica,
156 VT1000S, Leica Biosystems) were prepared from mice at the ages of P10 and P20 in ice-cold
157 oxygenated (95% O_2 - 5% CO_2) modified choline-based aCSF (in mM) 0.5 $CaCl_2$, 7 mM $MgSO_4$;

158 NaCl replaced by an equimolar concentration of choline). Slices were incubated for 30min at
159 32°C in an oxygenated normal aCSF containing (in mM): 126 NaCl, 3.5 KCl, 1.2 NaH_2PO_4, 26
160 $NaHCO_3$, 1.3 $MgCl_2$, 2.0 $CaCl_2$, and 10 D-glucose, pH 7.4, 315 mOsm/l. Slices were allowed to
161 equilibrate for at least 30 min at RT before being transferred to the recording chamber. During
162 recordings, slices were perfused at a rate of 4 ml/min with continuously aerated (95% O_2-5%
163 CO_2) normal aCSF at RT.
164 Data Acquisition: Neurons were impaled with patch pipettes (5–7 MΩ) and recorded in the
165 whole-cell configuration, either in the current-clamp or voltage-clamp mode. For current-clamp
166 experiments, the composition of the intracellular solution was: 130 mM K-$MeSO_4$, 5 mM KCl, 5
167 mM NaCl, 10 mM HEPES, 2.5 mM Mg-ATP, and 0.3 mM GTP, 265–275 mOsm, pH 7.3. For voltage-
168 clamp experiments, the composition of the intracellular solution was: 120 mM Cs-gluconate,
169 20mM CsCl, 0.1 mM $CaCl_2$, 1 mM EGTA, 0.4 mM Na-guanosine triphosphate, 2mM Mg-adenosine
170 triphosphate, 10 mM HEPES. No correction from liquid junction potential was applied between
171 the pipette and the aCSF. Whole-cell measurements were low-pass filtered at 5 kHz using an
172 Axopatch 200B amplifier (Molecular Devices, Inc). Recordings were digitized with the ITC-18
173 board (Instrutech, Inc) on a PC using custom-made codes in IgorPro (Wavemetrics, Inc). All
174 signals were collected at a sampling frequency of 20kHz.
175 Data Analysis: Data were analyzed using custom-written codes in IgorPro software
176 (Wavemetrics, Inc.). For passive membrane properties, the resting membrane potential (RMP,
177 mV) was measured within 3 min after establishing the whole-cell configuration, and monitored
178 throughout the experiment. To measure input resistance, a 500ms step-pulse protocol was used
179 with current stimulation from -200pA to +50pA. The input resistance (R_{in}, MΩ) was measured by
180 plotting the steady-state voltage deflection in an I-V plot and calculating the slope of the best fit
181 line curve (R_{in}=V/I). The τ_m (membrane time constant, ms) was obtained by fitting a single
182 exponential curve to the voltage deflection at -50pA, and the membrane capacitance (C_m) was
183 calculated using the formula $C_m = \tau_m/R_{in}$. In addition, the number of spikes generated in response
184 to a 500ms step-pulse range from +100pA to +300pA was measured.
185 To measure action potentials (APs) properties, we applied small supra-threshold 5ms step-pulse
186 currents to the cell from -65mV. The active properties were measured at the minimum current
187 stimulation (Rheobase, pA) that generated an AP. The AP threshold (mV) was calculated by
188 taking the first derivative of the voltage trace, defining a threshold and identifying the voltage
189 level at that time point. The rate of rise of the AP (dV/dt, mV/ms) was the maximum value of

190 that first derivative trace. The AP amplitude (mV) was defined as the voltage difference between
191 AP threshold and AP peak. The AP duration (ms) was calculated by the full width of the waveform
192 at the half maximal amplitude (half-width). The fast afterhyperpolarization (fAHP) minimum
193 (mV) was defined as the minimum voltage right after the AP. The fAHP amplitude (mV) was
194 calculated as the difference between the AHP minimum and the AP threshold. The fAHP time
195 (ms) was defined as the time duration from the time point of AP threshold to the fAHP minimum.
196 The composition of our intracellular solution resulted in chloride reversal potential of -60mV and
197 Na^+/K^+ reversal potential of +10mV. This allowed for measurements of spontaneous excitatory
198 postsynaptic currents (sEPSCs) to be recorded at -60mV and of spontaneous inhibitory
199 postsynaptic currents (sIPSCs) to be recorded at +10mV. Automatically selected events were
200 subsequently visually monitored to discard erroneously included noise. The events showing only
201 single peaks were selected for kinetics analysis. All currents detected from every single neuron
202 were averaged. The peak amplitude was calculated as the maximum current value. The time
203 constant of the decay phase was detected by curve fitting with a single exponential decay
204 function.
205
206 ***In vivo* extracellular recordings**
207 Surgery: Multisite extracellular recordings were performed in the PFC of P8–P10 (n=13) and P20–
208 P23 (n=14) C57/BL mice with both sexes. Mice were under urethane anesthesia (intraperitoneal
209 injection, 1 mg/g body weight; Sigma-Aldrich) before surgery. The bone over the mPFC (0.8 mm
210 anterior to bregma, 0.1–0.5 mm right to the midline) was carefully removed. One-shank
211 electrodes with 4 recording sites (0.4–0.8 MΩ impedance, 100 µm spacing, NeuroNexus) was
212 inserted into PFC at a depth of 1.9 mm from the skull surface. Electrodes were labelled with DiI
213 (1,1'-dioctadecyl-3,3,3',3'-tetramethyl indocarbocyanine; Invitrogen) to confirm their position
214 after histological assessment post-mortem. One silver wire was inserted into the cerebellum to
215 serve as ground and reference electrode.
216 Data Acquisition: A recovery period of 10 min following the insertion of electrodes before
217 acquisition of data was provided. Data acquired during the first 30 min of recording were used
218 for analysis to ensure similar state of anesthesia in all investigated pups. Extracellular signals
219 were bandpass filtered (0.1 Hz to 5 kHz) and digitized (32 kHz) with a multichannel extracellular
220 amplifier (Digital Lynx SX, Neuralynx) and the Cheetah acquisition software (Neuralynx).

221 Data Analysis: Data were imported and analyzed off-line using custom-written tools in MATLAB
222 software version 7.7 (MathWorks). Multiple unit activity (MUA) is detected when negative
223 deflections exceeding five times the SD of the bandpass filtered (500–5000 Hz) signals. Single
224 unit activity (SUA). SUA was detected and clustered using klusta (Rossant et al., 2016) and
225 manually curated using phy (https://github.com/cortex-lab/phy). Data were imported and
226 analyzed using custom-written tools in the MATLAB. Burst activity detection. Burst activity was
227 detected by using the method from (Gorin, Tsitoura et al. 2016). First, for each unit, Poisson
228 distribution, which assumed random independent spiking, was defined. The single parameter λ
229 of Poisson distribution is the average firing rate of the unit. Second, the median ISI value of the
230 Poisson distribution was derived. Third, we defined a burst activity as a sequence of ≥4
231 consecutive spikes separated by intervals smaller than the median ISI. Last, the percentage of
232 the burst activity of a single unit is calculated by 100* (the number of the burst activity / the
233 number of the spikes). A unit was classified as "burst unit" if >50% of all spikes occurred in bursts.
234

235 **Immunohistochemistry**

236 Mice at the age of P10 and P20 were perfused with 4% paraformaldehyde, followed by fixation
237 with the same solution for 1h at 4◦C, followed by cryoprotection and preparation of 12 µm
238 cryostat sections as previously described[88]. Primary antibodies used were rat monoclonal anti-
239 GFP (Nacalai Tesque, Kyoto, Japan, 1:5000), rabbit polyclonal anti-GFP (1:500; Minotech
240 biotechnology, Heraklion, Greece) and rabbit polyclonal anti- parvalbumin (PV) (Swant,
241 Bellinzona, Switzerland; 1:2000. Secondary antibodies used were goat anti-rat-Alexa Fluor-488,
242 goat anti-rabbit Alexa Fluor-488, and goat anti-rabbit-Alexa Fluor-555 (Molecular Probes,
243 Eugene, OR, United States, 1:800). Images were obtained with a confocal microscope (Leica TCS
244 SP2, Leica, Nussloch, Germany). For each age group (P10, P20), 2-4 10µm-thick sections from
245 each mouse brain were selected, all including the mPFC and BC.
246

247 **RNA *In Situ* Hybridization**

248 Non-radioactive *in situ* hybridization experiments were performed on cryostat sections (12µm
249 thick, see immunochemistry) according to the protocol described (Schaeren-Wiemers and
250 Gerfin-Moser 1993). Riboprobe was prepared by *in vitro* transcription and was specific
251 Somatostatin (SST) (Liodis et al. 2007).
252

253 **Nissl Staining**

254 Cryostat sections (12µm thick, see immunochemistry) were incubated in 1:1 100%
255 ethanol:chloroform overnight at RT. Then, sections were rehydrated for 1 min in 100%, 95%
256 ethanol solutions and dH_2O at RT, followed by a 10-min incubation in 0.1% cresyl violet solution
257 at 50°C. Sections were then dehydrated with dH_2O, 95%, 100% ethanol and xylene for 5 min and
258 coverslipped with permount. Images from whole sections were obtained in 5× magnification of
259 a light microscope (Axioskop 2FS, Carl Zeiss AG, 268 Oberkochen, Germany) and merged using
260 Adobe Photoshop CC 2015, Adobe Systems, Inc.

261

262 **Analysis for Immunochemistry, *in situ* hybridization and Nissl staining**

263 The background color of each cropped image was converted to black, while the cells were
264 colored blue. The images were loaded into Matlab, where the number of 'blue' pixels was
265 counted per area (mm^2). Each cell was assumed to be composed of four pixels. Therefore, the
266 number of cells was measured as the total number of 'blue' pixels divided by four
267 (Konstantoudaki et al. 2016; Chalkiadaki et, 2019). The results of the algorithm were double
268 checked with hand counting first, before applying the algorithm to multiple slices. An average
269 number was calculated for the number of neurons from mPFC and BC sections from each
270 developmental group.

271

272 **Western blots**

273 Mice were decapitated following cervical dislocation, the brain was quickly removed, placed in
274 ice cold PBS (phosphate-buffered saline) and then positioned on a brain mould, where 1.5 mm
275 slices were taken containing the mPFC and BC. The slices were placed on dry ice, and the
276 prelimbic area of mPFC was dissected out and stored at -80°C. The BC was also isolated from the
277 corresponding slices and stored at -80°C. Frozen tissue blocks were lysed in a solution containing
278 (in mM) HEPES 50, NaCl 150, MgCl2 1.5, EGTA 5, Glycerol 1%, Triton-X100 1%, 1:1000 protease
279 inhibitors cocktail. Proteins ran on 8.5% bis-acrylamide gel and were transferred onto a
280 nitrocellulose membrane (Whatman GmbH, Dassel, Germany). The membrane was blocked,
281 incubated in rabbit polyclonal anti-K+/Cl-Cotransporter (KCC2) (Merck KGaA, Darmstadt,
282 Germany, 1:1000) or rabbit monoclonal anti-GAPDH (Cell Signaling Technology Europe BV,
283 Leiden, Netherlands, 1:1000), washed, incubated in secondary goat anti-rabbit IgG Horseradish
284 Peroxidase Conjugate antibody (Invitrogen, 1:5000), and digitally exposed using the Molecular

285 Imaging system ChemiDoc (BioRad Laboratories, Inc, California, U.S.A.). Analysis of KCC2 and
286 GAPDH expression was performed with ImageJ software, and the raw values of KCC2 from each
287 sample were normalized to their respective GAPDH values.
288
289 **Statistical analysis**
290 Statistical analyses were performed in Microsoft Office Excel 2007 and GraphPad Prism Software
291 7.0. Data are presented as mean ± standard error of mean (SEM). Normality distribution and
292 equality of variances of dataset were tested with the Kolmogorov-Smirnov test normality test.
293 The null hypothesis was rejected for a >5%. When four experimental groups (P10 mPFC, P20
294 mPFC, P10 BC and P20 BC) were assessed and two variables were taken into consideration (age
295 and brain area), data were analyzed with a two-way ANOVA with Fisher LSD, Sidak's or Tukey's
296 multiple comparisons (electrophysiological recordings and cell counting). When three groups
297 (P10 mPFC, P20 mPFC and P10 BC) data were analyzed with one- way ANOVA
298 (electrophysiological recordings). For the comparison of *in vivo* spiking activity between P10 and
299 P20, statistical analyses were performed with MATLAB. Significant differences were detected by
300 one-way ANOVA. Significance levels of *p < 0.05, **p < 0.01, ***p < 0.001 or ****p < 0.0001
301 were tested. For comparison of Western blot analysis, the significant effect of each
302 developmental age group from mPFC and BC was assessed using Student's t-test depending on
303 the experiment.
304
305 **Data availability**
306 Data presented in the figures in this paper are available upon request.
307
308 **Results**
309 Mice belonging to two age groups were investigated: (i) neonatal mice included pups of
310 postnatal days (P) 9-11 and are defined as P10 while (ii) pre-juvenile mice defined as P20 animals
311 including pups of P19-P21. Due to the high density of intra-cortical synapses in the superficial
312 cortical layers (DeFelipe and Fariñas 1992; Clancy et al. 2001) and their specific involvement in
313 neurodevelopmental disorders (Chini and Hanganu-Opatz, 2020; Bitzenhofer eta l., 2017) we
314 focused on the superficial layers of the mPFC and BC. From each mouse brain, both the mPFC
315 and the BC were studied. All analyses that had four groups (mPFC P10 and P20, BC P10 and P20)

316 were conducted using two-way ANOVA, with the two factors being the brain area (mPFC and
317 BC) and age (P10 and P20).
318
319 **Synaptic transmission decreased in mPFC and BC across development**
320 First, we investigated the synaptic properties of mPFC and BC in neonatal compared to juvenile
321 mice. We measured basal synaptic transmission using extracellular field recordings in brain
322 slices. The evoked field excitatory postsynaptic potentials (fEPSPs) in layer II/III of both areas
323 were recorded in response to current pulses of increasing intensity through the stimulating
324 electrodes in layer II/III (**Figure 1a,c**). The fEPSPs were significantly decreased in both mPFC and
325 BC at P20 compared to P10 (**Figure 1b,d**).
326 The decreased fEPSP responses at P20, compared to P10 (**Figure 1b,d**), could result from
327 either increased inhibitory postsynaptic currents or decreased excitatory postsynaptic currents.
328 To examine this, we performed patch-clamp recordings from layer II/III pyramidal neurons in
329 mPFC and BC from P10 and P20 mice. We recorded spontaneous inhibitory postsynaptic currents
330 (sIPSCs, at +10mV) and spontaneous excitatory postsynaptic currents (sEPSCs, at -60mV) and we
331 measured the frequency, amplitude and decay time constant.
332 In mPFC, the frequency of sIPSCs was significantly augmented at P20 compared to P10
333 (**Figure 2a,b**), while the sIPSC amplitude and decay-time constant did not significantly change
334 over the investigated time window (**Figure 2a,c,d**). The sIPSC frequency remained increased at
335 P20, compared to P10, in the presence of AMPA and NMDA receptor antagonists, CNQX and AP5,
336 respectively. On the other hand, bicuculine, a $GABA_A$ receptor antagonist, blocked the sIPSCs
337 both in P10 and P20 mPFC (Supplemental Figure 1). In BC, sIPSC frequency and amplitude were
338 significantly increased, at P20 compared to P10 (**Figure 2a,b,c**), while the decay-time constant
339 was not altered (**Figure 2a,d**). When comparing the two brain areas, we noticed a significantly
340 lower sIPSC frequency in the mPFC compared to BC at both ages (**Figure 2a,b**). The decay time
341 constant was similar (**Figure 2a,d**), while the sIPSC amplitude was significantly smaller at P20 in
342 the mPFC compared to BC (**Figure 2a,c**).
343 The sEPSC frequency was significantly decreased at P20 compared to P10, in both areas
344 (**Figure 2e,f**), while the amplitude and decay time constant were unaltered (**Figure 2e,g,h**).
345 However, in the presence of bicuculine (10uM) the sEPSC frequency was reduced at mPFC P10
346 and was not different between P20 and P10 mPFC (Supplemental Figure 1). Upon comparing the
347 two brain areas, the sEPSC frequency and amplitude were found significantly decreased in mPFC,

348 compared to BC, at P10 (**Figure 2e,f**). At P20, the sEPSC frequency was similar between the two
349 cortical areas, while the amplitude remained significantly smaller in mPFC compared to BC in
350 both ages (**Figure 2e,g**). The decay time constant was not different between areas at both ages
351 (**Figure 2e, h**).
352 The increased sIPSC frequency can underlie the fEPSP reduction from P10 to P20 in mPFC
353 and BC (**Figure 1b,d**). In addition, specifically for mPFC, the possibility for the presence of $GABA_A$-
354 mediated sEPSCs could also contribute to the fEPSP reduction from P10 to P20.
355
356 **Passive and active membrane properties of MGE-derived interneurons are altered in the mPFC**
357 **across development**
358 Changes in interneuron properties could underlie the increased sIPSC frequency. To investigate
359 this, we performed current-clamp recordings from layer II/III mPFC and BC of $Lhx6^+$ interneurons.
360 For this reason, Lhx6-cre;ROSA26fl-STOP-fl-YFP mice were used in which $Lhx6^+$ interneurons
361 express YFP. Lhx6 is expressed by all post-mitotic and mature MGE-derived interneurons (Liodis
362 et al. 2007), therefore, YFP is expressed in MGE-derived interneurons, which include
363 interneurons that express parvalbumin (PV^+) and somatostatin (SST^+).
364 Upon analysis of the passive properties, we found a significant increase in the input resistance
365 and membrane time constant, as well as a significant decrease in the membrane capacitance in
366 the mPFC at P10 compared to P20. In addition, the input resistance and the membrane time
367 constant were higher at P10 mPFC, compared to BC (P10 and P20). There was no difference in
368 the resting membrane potential (RMP) between ages and brain areas (**Figure 3, Supplementary**
369 **Table 1**).
370 With regard to the active properties, there was no significant difference between ages and brain
371 areas in the AP amplitude, AP threshold, rheobase and fAHP time (Figure 4a, d, e, g;
372 **Supplementary Table 1**). The AP rate of rise (dv/dt) was significantly increased while the AP
373 duration (half-width) was significantly reduced at P20 compared to P10 in both the mPFC and
374 BC (**Figure 4b-c, Supplementary Table 1**). In addition, the fAHP amplitude was significantly lower
375 in the mPFC (**Figure 4f, Supplementary Table 1**), compared to BC. The increased rate of rise and
376 the decreased AP duration are possibly linked with the up-regulation of voltage-dependent
377 sodium channels during development (Huguenard et al. 1988), and in combination with the
378 reduced fAHP amplitude suggest that the mPFC MGE-interneurons at P10 are still quite

379 immature, when compared to adult PV^+/SST^+ interneurons in mPFC (Yang et al. 2013; Pan et al.
380 2017).
381 Overall, these data indicate that some intrinsic properties of interneurons in mPFC change with
382 age (from P10 to P20), reaching values that closer resemble adult MGE-derived interneurons
383 (Yang et al. 2013; Pan et al. 2017). Therefore, the increased sIPSC frequency of mPFC pyramidal
384 neurons observed at P20, compared to P10 could partly be explained by these altered properties
385 of presynaptic interneurons.
386
387 **The emergence of PV immunoreactivity is delayed in mPFC compared to BC**
388 An additional explanation for the increased sIPSC frequency could come from alterations in
389 interneuron cell densities. To test this, we quantified the number of interneurons per area in
390 cryosections at P10 and P20 mPFC and BC coronal brain slices of $Lhx6^+$-expressing mice. The YFP^+
391 positive cells per area (i.e. $Lhx6^+$ cell density) in mPFC and BC was similar between ages, but was
392 significantly lower in the mPFC, compared to BC (**Figure 5a**). The percentage of cell death in
393 $Lhx6^+$ neurons is very low in both P10 mPFC and BC (**Supplementary Figure 2**).
394 The transcription factor Lhx6 is required for the specification and maintenance of main MGE-
395 derived interneurons, PV and SST-positive interneuron subtypes, at postnatal ages (Liodis et al.
396 2007). The neuropeptide SST (both mRNA and protein) is progressively expressed from
397 embryonic to postnatal levels (Bendotti et al. 1990; Forloni et al. 1990). We found that the SST
398 mRNA levels were similar between areas and ages (**Figure 5b**). On the other hand, the
399 emergence of PV immunoreactivity in the mouse cortex shows a delayed development, starting
400 from early postnatal period to adult, with marked area-specific differences(Del Rio et al. 1992).
401 We found that PV was only immunoreactive in BC, and not in mPFC, at P10 (**Figure 5c and**
402 **Supplementary Figure 3 and 4**). At P20, PV was immunoreactive in both mPFC and BC, but PV^+
403 cell density was significantly lower in the mPFC, compared to BC (**Figure 5c and Supplementary**
404 **Figure 3 and 4**).
405 We also counted the total cell density of mPFC and BC from neonatal and juvenile mice
406 (**Supplementary Figure 5a**) using Nissl staining. In the mPFC, the cell density significantly
407 decreased at P20 compared to P10 (**Supplementary Figure 5b**). On the contrary, in BC, the total
408 cell density significantly increased at P20 compared to P10 (**Supplementary Figure 5b**). When
409 the two brain areas were compared, no difference was found at P10, while the mPFC cell density
410 was significantly lower compared to BC at P20 (**Supplementary Figure 5b**).

411 We further examined whether the alterations in total cell density are derived from alterations
412 in cell density of interneurons by measuring the Lhx6$^+$ neurons over the Nissl-positive cells. No
413 differences were detected between areas and ages (**Supplementary Figure 5c).** These results
414 suggest that the changes in total cell density in mPFC and BC respectively are probably due to
415 changes in other neuronal or glial populations.
416
417 **GABA is depolarizing in the neonatal mPFC but not BC**
418 Our data so points at several similarities in the development of mPFC and BC from the neonatal
419 to pre-juvenile period, but also indicates a protracted maturation of several mPFC interneuron
420 properties (intrinsic properties and PV immunoreactivity). Therefore, it is likely that another
421 GABAergic developmental process occurs at a later time point in the mPFC, and specifically, that
422 of the switch from depolarizing to hyperpolarizing function of $GABA_AR$. It is well known that
423 $GABA_AR$ is depolarizing during the first postnatal week, but switches to hyperpolarizing at P7 in
424 the hippocampus, cortex and amygdala (Ben-Ari et al. 1989; Luhmann and Prince 1991; LoTurco
425 et al. 1995; Owens et al. 1996; Martina et al. 2001; Gulledge and Stuart 2003; Ben-Ari et al. 2007;
426 Kirmse et al. 2015). Therefore, at P10, $GABA_AR$ function is inhibitory in the BC. We used
427 diazepam (2µM) (a $GABA_AR$ agonist) to enhance $GABA_AR$ function and determine whether it is
428 depolarizing by measuring the fEPSP response. At P10, diazepam did not significantly alter the
429 fEPSP in BC, as expected if $GABA_AR$ function is inhibitory. However, diazepam increased the
430 fEPSP amplitude in mPFC at P10 (**Figure 6a-b**). At P20, the fEPSP amplitude was not significantly
431 altered following diazepam application in both mPFC and BC (**Figure 6c,d**). The fEPSP
432 enhancement was also evident in the presence of AMPA and NMDA receptor antagonists (CNQX
433 and AP5) (Supplementary Figure 6a-c). These results suggest that the $GABA_AR$ function is
434 depolarizing in the mPFC at P10.
435 The switch in the $GABA_AR$ function from depolarizing to hyperpolarizing occurs due to the
436 increased expression of the K^+-Cl^- co-transporter 2 (KCC2) (Rivera et al. 1999). To determine
437 whether modulating chloride transporters could alter the diazepam-induced enhancement of
438 the fEPSP, we recorded the fEPSP in the presence of bumetanide (10uM), which blocks the
439 NKCC1 transporter, and tested the effect of diazepam. We find that in the presence of
440 bumetanide, diazepam did not result in an increase of the fEPSP (Supplementary Figure 6). In
441 addition, we measured KCC2 protein levels and demonstrated that they were significantly
442 increased at P20 compared to P10 in the mPFC but not in the BC (**Figure 7a,b**). These results

443 further support our hypothesis that the $GABA_AR$ function is depolarizing at P10 in the mPFC and
444 could explain the observed increased fEPSPs, sEPSC frequency and decreased sIPSCs.
445
446 **No significant changes in pyramidal neuron excitability**
447 To determine whether the reduced sEPSC frequency can be explained by changes in pyramidal
448 neuron excitability, we investigated their intrinsic properties. The passive and active properties
449 of these neurons were measured using current-clamp recordings from layer II/III mPFC and BC
450 pyramidal neurons. With regards to passive properties, no significant differences were observed
451 in the RMP, the input resistance and the membrane time constant between brain regions and
452 ages (**Supplementary Figure 7, Supplementary Table 1**). Only the membrane capacitance was
453 significantly increased at P20 compared to P10 (**Supplementary Figure 7d, Supplementary Table**
454 **1**), in both brain areas. In addition, the number of spikes generated with increasing current
455 stimulation was not significantly different between ages and regions (**Supplementary Figure 8**).
456 In terms of active properties, the AP amplitude and rate of rise were increased at P20 compared
457 to P10 mPFC, while the AP half-width, rheobase and threshold were not significantly different
458 (**Figure 8, Supplementary Table 1**). The AP amplitude was also significantly increased at P20,
459 compared to P10 in BC, while the other properties did not change (**Figure 8, Supplementary**
460 **Table 1**). Comparing the two regions at the two ages, we found no significant differences of AP
461 properties of pyramidal neurons (**Figure 8, Supplementary Table 1**). The developmental increase
462 of AP amplitude and rate of rise in the mPFC could be due to the on-going maturation of sodium
463 channels in pyramidal neurons. However, these changes could not account for the reduced
464 sEPSCs in the neonatal, compared to pre-juvenile, mPFC and BC.
465
466 **Diazepam-modulated spontaneous activity in mPFC brain slices of neonatal mice**
467 To understand how network activity is affected in the neonatal mPFC compared to the juvenile
468 mPFC, we initially recorded spontaneous activity in mPFC brain slices. We find that spontaneous
469 activity events are significantly increased in the juvenile mPFC compared to the neonatal mPFC
470 (Figure 9a,b). On the other hand, there is no difference in the number of spontaneous activity
471 events between P10 and P20 in the BC (Figure 9a,b). Furthermore, the addition of diazepam
472 increased the number of spontaneous activity events by 100% compared to control conditions
473 at P10 in the mPFC (Figure 9Cc,d). The diazepam-induced change was significantly less at P20
474 mPFC, compared to P10 (Figure 9c,d). The concurrent administration of bumetanide (antagonist

475 of sodium-potassium-chloride (Na-K-Cl) cotransporters, NKCC1) and diazepam actually reduced
476 the number of spontaneous events at P10 mPFC (50% less). This percent change was significantly
477 less compared to the % change at P20 mPFC (Figure 9). We suggest that the spontaneous activity
478 of early mPFC networks (P10) modulated by the excitatory action of $GABA_A$ R in combination
479 with (Na-K-Cl) cotransporters.
480
481 **Increased firing activity *in vivo* in the mPFC between the second and third postnatal weeks**
482 To investigate the physiological network activity *in vivo*, multisite recordings of the LFP and
483 multi-unit activity (MUA) were performed in layers II/III of mPFC at P8-10 and P20-23. A
484 significant increase of MUA was identified at P22 compared to P9 mice, indicating a
485 developmental increased spiking activity in layers II/III of mPFC on the third compared to the
486 second postnatal week (Figure 10). Similarly, the spiking activity in the BC augmented with age
487 (Supplementary Figure 9). To characterize the firing dynamics along development, we used MUA
488 for clustering single-unit activity. We detected bursts of spikes using the previously developed
489 method (Gorin et al. 2016). The burst occurrence in the mPFC increased with age (33.62±1.91
490 %, 161 single units at neonatal age vs. 50.12±4.91 %, 150 single units at pre-juvenile age;
491 $p<0.0001$, One-way ANOVA, $F_{(1, 309)}=272.26$). Correspondingly, the number of units organized in
492 bursts increased with age too from 21 out of 161 single units at neonatal age to 104 out of 150
493 single units at pre-juvenile age (Figure 10d). Moreover, we analyzed the mPFC and BC units in
494 their amplitude, dv/dt and half-width and detected, similarly to the in vitro conditions, a
495 significant increase in the AP amplitude and rate of rise but no difference in the half-width
496 (Supplementary Figure 10). These results provide further evidence that the decreased excitatory
497 synaptic activity of mPFC cannot be attributed to increased spiking activity of mPFC neurons at
498 P10.
499
500 **Discussion**
501 Our study has identified significant developmental events in the mPFC and the BC between the
502 second and third postnatal weeks. Specifically, we have shown that the basal synaptic
503 transmission decreases from the second to the third postnatal week, a fact that can be explained
504 by an increase in the sIPSCs in both mPFC and BC. Moreover, our data support a depolarizing
505 action of $GABA_AR$ in the second postnatal week, in the mPFC only and not the BC, as indicated
506 by the presence of non-AMPA-mediated sEPSCs, increased basal synaptic transmission following

507 $GABA_AR$ activation, which is blocked by concurrent bumetanide application, and decreased
508 protein levels of KCC2. In parallel, differences in the development of the intrinsic properties of
509 GABAergic interneurons from the neonatal to juvenile period were identified between the mPFC
510 and BC. Finally, the AP amplitude and AP rate-of-rise of pyramidal cells also change with age and
511 relate to augmented network activity across development, both *in vitro* and *in vivo*.
512
513 **Depolarizing action of GABA in the immature cortex**
514 GABA plays a crucial role in inhibiting adult neurons, acting primarily via the chloride-permeable
515 $GABA_AR$ and resulting in hyperpolarization of the membrane potential (Kaila and Voipio 1987).
516 However, GABA action leads to depolarization of immature neurons (i.e. during the first
517 postnatal week in mice), due to an initially higher intracellular chloride concentration $[Cl^-]_{in}$ (Ben-
518 Ari 2001; Ben-Ari et al. 2007; Ben-Ari 2012). The developmental switch of GABA action from
519 depolarizing to hyperpolarizing results from changes in cation-chloride co-transporter
520 expression: NKCC1, a cation-Cl^- importer, is highly expressed in neuronal precursor cells during
521 early brain development (Plotkin et al. 1997; Yamada et al. 2004), while the expression of the
522 K^+-Cl^- cotransporter 2 (KCC2), a cation-Cl^- exporter, increases after the first postnatal week (Ben-
523 Ari 2001; Ben-Ari et al. 2007; Ben-Ari 2012). This increased KCC2 transporter expression might
524 provide a central mechanism for the depolarization to hyperpolarization switch of GABAergic
525 transmission via progressive reduction of $[Cl^-]_{in}$ (Lu et al. 1999; Rivera et al. 1999; Ganguly et al.
526 2001; Ben-Ari 2002; Dzhala et al. 2005; Fiumelli et al. 2005).
527 The $GABA_AR$ switch from depolarizing to hyperpolarizing occurs at P7 in the hippocampus,
528 cortex, amygdala (Ben-Ari et al. 1989; Luhmann and Prince 1991; LoTurco et al. 1995; Owens et
529 al. 1996; Martina et al. 2001; Gulledge and Stuart 2003; Ben-Ari et al. 2007). Our study suggests
530 that this switch is delayed in the mPFC compared to primary somatosensory cortex and it takes
531 place between P10 and P20. Specifically, we show that increased $GABA_AR$ activity leads to
532 enhanced fEPSPs in neonatal mPFC (P10), suggesting that the $GABA_AR$ function is depolarizing in
533 the mPFC at P10. This enhancement is prevented in the presence of the NKCC1 blocker,
534 bumetanide. Furthermore, diazepam increases the number of spontaneous activity events in the
535 brain slice, which is also prevented in the presence of bumetanide. This hypothesis is further
536 supported by decreased levels of KCC2 transporter in the neonatal mPFC. Our results could have
537 implications for understanding the protracted maturation of mPFC compared to other cortical

538 areas, which may depend on a combination of a delayed switch from depolarizing-to-
539 hyperpolarizing function of $GABA_AR$ and maturation of interneurons.
540
541 **Interneurons and mPFC development**
542 Recordings of $Lhx6^+$- interneurons indicate that both passive and active properties are regulated
543 by age and reach values that better resemble adult MGE-derived interneurons. Specifically, we
544 have found that the input resistance and AP width decrease while the AP rate of rise increases
545 in the mPFC at P20 compared to P10. In part, similar findings have been identified for PV^+ cells
546 in the hippocampus (Doischer et al. 2008; Miyamae et al. 2017) and SST^+ cells in the anterior
547 cingulate cortex (Pan et al. 2017). On the other hand, the AHP amplitude is still quite immature
548 in the mPFC at P20, compared to PV^+, SST^+ interneurons in primary sensory areas or the
549 hippocampus and compared to adult mPFC (Doischer et al. 2008; Yang et al. 2013; Pan et al.
550 2017). Therefore, it is likely that the physiological properties of PV+ and SST+ interneurons in
551 the mPFC continue to change past the third postnatal week.
552 Our knowledge on the neonatal physiology of mPFC GABAergic interneurons is very limited. It
553 has been shown that PV expression is lowest in juveniles and increases during adolescence to
554 levels similar to those observed in adulthood (Caballero et al. 2014). Furthermore, PV expression
555 is not evident in the neonatal period and emerges during the pre-juvenile period in the mPFC
556 (del Rio et al. 1994; de Lecea et al. 1995; Zheng et al. 2011; Spampanato and Sullivan 2016). Our
557 results agree with these findings, as PV expression was detected in very low amounts during the
558 pre-juvenile period in the mPFC.
559 In addition, our study has identified decreased excitatory and increased inhibitory synaptic
560 function between the second and third postnatal weeks. We show that the frequency of sIPSCs
561 in layer II/III pyramidal cells of mPFC increases from neonatal to pre-juvenile period, consistent
562 with the developmental changes of IPSCs in layer III pyramidal neurons of monkey PFC
563 (González-Burgos et al. 2015) and mouse mPFC (Kroon et al. 2019).
564
565 **Pyramidal neurons and network activity**
566 It has been suggested that spontaneous network activity changes from local, highly synchronized
567 to more diffuse from the second to the third postnatal weeks, in the primary sensory cortices
568 (Golshani et al. 2009; Frye and MacLean 2016). Oscillatory activity in the mPFC first emerges at

569 P15 (Bitzenhofer et al. 2019). In this study, we have found increased spiking activity in the mPFC
570 during the third, compared to the second postnatal week. This occurred despite the decreased
571 excitatory and increased inhibitory synaptic function, but could be explained partly by the
572 developmental increase of AP amplitude and rate of rise in the mPFC layer II/III pyramidal
573 neurons, which could be due to the on-going maturation of sodium channels in pyramidal
574 neurons.
575 Studies in developing mPFC pyramidal neurons have proposed that there is a unique sensitive
576 time window for synaptic maturation of these neurons from individual cortical layers. During rat
577 mPFC layer V development, the intrinsic properties, synaptic inputs and morphology of
578 pyramidal neurons develop together during early postnatal life. While the greatest changes were
579 reported during the first ten days after birth, the adult-like properties emerged after the end of
580 the third week (P21) (Zhang et al. 2011). This study confirms that the second postnatal week is
581 a period of rapid growth, similar to that in other neocortical regions by combining functional and
582 structural measurements of developing pyramidal neurons in mouse mPFC (Zhu 2000; Romand
583 et al. 2011).
584
585 **Developmental PFC malformation leads to cognitive disorders in adulthood**
586 The neonatal functional maturation of GABAergic circuits and E/I (excitation to inhibition)
587 balance are critical for PFC-dependent behaviours and plasticity in the adult while their
588 malfunction leads to many psychiatric disorders (Benes 1991; Kilb 2012; Ferguson and Gao
589 2018). From the prenatal period to late adolescence, the PFC network is highly vulnerable to
590 genetic and environmental factors (Andersen 2003), since the mPFC is one of the latest cortical
591 regions to develop (Huttenlocher 1990). While many studies have focused on understanding
592 several developmental processes during adolescence (Caballero et al. 2016), our knowledge
593 regarding the ongoing cellular and network developmental processes during the perinatal period
594 is notably limited, despite significant evidence showing that environmental manipulations
595 during this period manifest as complex psychiatric and neurologic disorders in adulthood
596 (Weinberger 1986).
597 The delayed developmental shift of GABA action in various mouse models mimicking human
598 brain disorders have been investigated, including the maternal immune activation model
599 (Corradini et al. 2018; Fernandez et al. 2018), the Scn1a and Scn1b mouse models of Dravet
600 syndrome (Yuan et al., 2019), the 22q11.2 deletion syndrome (Amin et al. 2017) and the Fmr1

601 deficient model of fragile X syndrome (He et al. 2018). In the latter study, early postnatal
602 correction of GABA depolarization (bumetanide-treated) led to sufficient normalization of the
603 mature BC network (He et al. 2018). The impaired KCC2 has been proposed as a potential
604 therapeutic target of epilepsies by many studies in animal models and human patients (Moore
605 et al. 2017).

606 Our study focuses in understanding the early developmental cellular and physiological
607 mechanisms of mPFC circuits, before adolescence, and proposes that the neonatal mPFC
608 compared to BC exhibits a delayed switch from depolarization to hyperpolarization function of
609 $GABA_AR$. Our results raise the possibility that the delayed maturation of mPFC compared to other
610 cortical areas depends on a combination of a delayed switch from depolarization to
611 hyperpolarization function of the $GABA_AR$ and delayed maturation of interneurons.

612

613 **Acknowledgements:**

614 Authors are grateful to Emmanuella Foinikianaki for her help with Matlab analysis and histology
615 and to Giasemi Eptaminitaki for her help in *in situ* hybridization experiments. They also would
616 like to thank all the members of Karagogeos and Sidiropoulou Labs and the animal facility of the
617 IMBB for help with experiments. This study was co-financed through the Operational Program
618 "Education and Lifelong Learning" of the National Strategic Reference Framework – Research
619 Funding Program (EDBM34) by a grant to DK (10040) and through the BIOIMAGING-GR, National
620 Roadmap for Research Infrastructures from the European Union (European Social Fund-ESF) and
621 Greek National Funds. KK has been a recipient of the Manasaki fellowship and a Medical School
622 fellowship of the University of Crete and a poster award at the 27th Hellenic Society for
623 Neuroscience Meeting.

624 **Author Contributions:**

625 All experiments were conceived and designed by K.K., K.S., and D.K. All experiments performed
626 by K.K., A.V., O.C. and X.X. Data were analyzed by K.K., A.V., O.C., M.D. K.S. and discussed with
627 D.K. X.X. and I.L.H.-O. X.X. carried out and analyzed the *in vivo* experiments. Manuscript was
628 written by K.K., D.K. and K.S. All authors discussed and commented on the manuscript.

629

630 **References:**

631 Allene C, Cattani A, Ackman JB, Bonifazi P, Aniksztejn L, Ben-Ari Y, Cossart R. 2008. Sequential
632 Generation of Two Distinct Synapse-Driven Network Patterns in Developing Neocortex. J
633 Neurosci. 28:12851–12863.
634 Amin H, Marinaro F, De Pietri Tonelli D, Berdondini L. 2017. Developmental excitatory-to-
635 inhibitory GABA-polarity switch is disrupted in 22q11.2 deletion syndrome: a potential
636 target for clinical therapeutics. Scientific Reports. 1–18.
637 Andersen SL. 2003. Trajectories of brain development: point of vulnerability or window of
638 opportunity? Neuroscience & Biobehavioral Reviews. 27:3–18.
639 Bahrey HLP, Moody WJ. 2003. Early Development of Voltage-Gated Ion Currents and Firing
640 Properties in Neurons of the Mouse Cerebral Cortex. Journal of Neurophysiology. 89:1761–
641 1773.
642 Bartolini G, Ciceri G, Marin O. 2013. Integration of GABAergic Interneurons into Cortical Cell
643 Assemblies: Lessons from Embryos and Adults. 79:849–864.
644 Ben-Ari Y. 2001. Developing networks play a similar melody. Trends in Neurosciences. 24:353–
645 360.
646 Ben-Ari Y. 2002. Excitatory actions of gaba during development: the nature of the nurture. Nat
647 Rev Neurosci. 3:728–739.
648 Ben-Ari Y. 2012. Refuting the challenges of the developmental shift of polarity of GABA actions:
649 GABA more exciting than ever! 1–18.
650 Ben-Ari Y, Cherubini E, Corradetti R, Gaiarsa JL. 1989. Giant synaptic potentials in immature rat
651 CA3 hippocampal neurones. The Journal of Physiology. 416:303–325.
652 Ben-Ari Y, Gaiarsa JL, Tyzio R, Khazipov R. 2007. GABA: A Pioneer Transmitter That Excites
653 Immature Neurons and Generates Primitive Oscillations. Physiological Reviews. 87:1215–
654 1284.
655 Ben-Ari Y, Khalilov I, Kahle KT, Cherubini E. 2012. The GABA Excitatory/Inhibitory Shift in Brain
656 Maturation and Neurological Disorders. The Neuroscientist. 18:467–486.
657 Bendotti C, Hohmann C, Forloni G, Brain RRD, 1990. 1990. Developmental expression of
658 somatostatin in mouse brain. II. In situ hybridization. Elsevier. 53:26–39.
659 Benes FM. 1991. Deficits in Small Interneurons in Prefrontal and Cingulate Cortices of
660 Schizophrenic and Schizoaffective Patients. Archives of General Psychiatry. 48:996–1001.

661 Best JR, Miller PH. 2010. A Developmental Perspective on Executive Function. Child
662 Development. 81:1641–1660.
663 Bitzenhofer SH, Ahlbeck J, Wolff A, Wiegert JS, Gee CE, Oertner TG, Hanganu-Opatz IL. 2017.
664 Layer-specific optogenetic activation of pyramidal neurons causes beta-gamma entrainment
665 of neonatal networks. Nature Communications. 8:14563.
666 Bitzenhofer SH, Poepplau JA, Chini M, Marquardt A, Hanganu-Opatz I. 2019. Activity-dependent
667 maturation of prefrontal gamma oscillations sculpts cognitive performance. bioRxiv. 1–39.
668 Bitzenhofer SH, Sieben K, Siebert KD, Spehr M, Hanganu-Opatz IL. 2015. Oscillatory Activity in
669 Developing Prefrontal Networks Results from Theta-Gamma-Modulated Synaptic Inputs.
670 CellReports. 11:486–497.
671 Brockmann MD, Pöschel B, Cichon N, Hanganu-Opatz IL. 2011. Coupled Oscillations Mediate
672 Directed Interactions between Prefrontal Cortex and Hippocampus of the Neonatal Rat.
673 Neuron. 71:332–347.
674 Burgard EC, Hablitz JJ. 1993. Developmental changes in NMDA and non-NMDA receptor-
675 mediated synaptic potentials in rat neocortex. Journal of Neurophysiology. 69:230–240.
676 Caballero A, Flores-Barrera E, Cass DK, Tseng KY. 2014. Differential regulation of parvalbumin
677 and calretinin interneurons in the prefrontal cortex during adolescence. Brain Struct Funct.
678 219:395–406.
679 Caballero A, Granberg R, Tseng KY. 2016. Mechanisms contributing to prefrontal cortex
680 maturation during adolescence. Neuroscience & Biobehavioral Reviews. 1–29.
681 Casey BJ, Giedd JN, Thomas KM. 2000. Structural and functional brain development and its
682 relation to cognitive development. Biological Psychology. 54:241–257.
683 Chalkiadaki K, Velli A, Kyriazidis E, Stavroulaki V, Vouvoutsis V, Chatzaki E, Aivaliotis M,
684 Sidiropoulou K. 2019. Development of the MAM model of schizophrenia in mice: Sex
685 similarities and differences of hippocampal and prefrontal cortical function.
686 Neuropharmacology 144, 193–207.
687 Chini, M. & Hanganu-Opatz, I. L. 2020. Prefrontal Cortex Development in Health and Disease:
688 Lessons from Rodents and Humans. *Trends Neurosci*
689 Clancy B, Darlington RB, Neuroscience BF, 2001. 2001. Translating developmental time across
690 mammalian species. Elsevier. 105:7–17.
691 Corradini I, Focchi E, Rasile M, Morini R, Desiato G, Tomasoni R, Lizier M, Ghirardini E, Fesce R,
692 Morone D, Barajon I, Antonucci F, Pozzi D, Matteoli M. 2018. Maternal Immune Activation

693 Delays Excitatory-to-Inhibitory Gamma-Aminobutyric Acid Switch in Offspring. Biological
694 Psychiatry. 83:680–691.
695 de Lecea L, del Ri o JA, Soriano E. 1995. Developmental expression of parvalbumin mRNA in the
696 cerebral cortex and hippocampus of the rat. Molecular Brain Research. 32:1–13.
697 DeFelipe J, Fariñas I. 1992. The pyramidal neuron of the cerebral cortex: Morphological and
698 chemical characteristics of the synaptic inputs. Progress in Neurobiology. 39:563–607.
699 del Rio J, De Lecea L, Ferrer I, Soriano E. 1994. The development of parvalbumin-
700 immunoreactivity in the neocortex of the mouse. 81:247–259.
701 Del Rio JA, Soriano E, Ferrer I. 1992. Development of GABA-immunoreactivity in the neocortex
702 of the mouse. J Comp Neurol. 326:501–526.
703 Diamond A. 2005. Normal Development of Prefrontal Cortex from Birth to Young Adulthood:
704 Cognitive Functions, Anatomy, and Biochemistry. In: Principles of Frontal Lobe Function.
705 Oxford University Press. p. 466–503.
706 Doischer D, Aurel Hosp J, Yanagawa Y, Obata K, Jonas P, Vida I, Bartos M. 2008. Postnatal
707 Differentiation of Basket Cells from Slow to Fast Signaling Devices. J Neurosci. 28:12956–
708 12968.
709 Dzhala VI, Talos DM, Sdrulla DA, Brumback AC, Mathews GC, Benke TA, Delpire E, Jensen FE,
710 Staley KJ. 2005. NKCC1 transporter facilitates seizures in the developing brain. Nature
711 Medicine 2005 11:11. 11:1205–1213.
712 Ferguson BR, Gao W-J. 2018. PV Interneurons: Critical Regulators of E/I Balance for Prefrontal
713 Cortex-Dependent Behavior and Psychiatric Disorders. Front Neural Circuits. 12:479–13.
714 Fernandez A, Dumon C, Guimond D, Tyzio R, Bonifazi P, Lozovaya N, Burnashev N, Ferrari DC,
715 Ben-Ari Y. 2018. The GABA Developmental Shift Is Abolished by Maternal Immune Activation
716 Already at Birth. Cerebral Cortex. 130:e1447–11.
717 Fiumelli H, Cancedda L, Poo M-M. 2005. Modulation of GABAergic Transmission by Activity via
718 Postsynaptic Ca2+-Dependent Regulation of KCC2 Function. Neuron. 48:773–786.
719 Forloni G, Hohmann C, Research JCDB, 1990. 1990. Developmental expression of somatostatin
720 in mouse brain. I. Immunocytochemical studies. Elsevier. 53:6–25.
721 Frye CG, MacLean JN. 2016. Spontaneous activations follow a common developmental course
722 across primary sensory areas in mouse neocortex. Journal of Neurophysiology. 116:431–
723 437.
724 Fuster J. 2015. The Prefrontal Cortex. Academic Press.

725 Ganguly K, Schinder AF, Wong ST, Poo M-M. 2001. GABA Itself Promotes the Developmental
726 Switch of Neuronal GABAergic Responses from Excitation to Inhibition. Cell. 105:521–532.
727 Golshani P, Goncalves JT, Khoshkhoo S, Mostany R, Smirnakis S, Portera-Cailliau C. 2009.
728 Internally Mediated Developmental Desynchronization of Neocortical Network Activity. J
729 Neurosci. 29:10890–10899.
730 Gorin, M., C. Tsitoura, A. Kahan, K. Watznauer, D. R. Drose, M. Arts, R. Mathar, S. O'Connor, I. L.
731 Hanganu-Opatz, Y. Ben-Shaul and M. Spehr (2016). "Interdependent Conductances Drive
732 Infraslow Intrinsic Rhythmogenesis in a Subset of Accessory Olfactory Bulb Projection
733 Neurons." The Journal of Neuroscience 36(11): 3127-3144.
734 González-Burgos G, Miyamae T, Pafundo DE, Yoshino H, Rotaru DC, Hoftman G, Datta D, Zhang
735 Y, Hammond M, Sampson AR, Fish KN, Bard Ermentrout G, Lewis DA. 2015. Functional
736 Maturation of GABA Synapses During Postnatal Development of the Monkey Dorsolateral
737 Prefrontal Cortex. Cerebral Cortex. 25:4076–4093.
738 Gulledge AT, Stuart GJ. 2003. Excitatory Actions of GABA in the Cortex. Neuron. 37:299–309.
739 Guo ZV, Li N, Huber D, Ophir E, Gutnisky D, Ting JT, Feng G, Svoboda K. 2014. Flow of Cortical
740 Activity Underlying a Tactile Decision in Mice. Neuron. 81:179–194.
741 He Q, Arroyo ED, Smukowski SN, Xu J, Piochon C, Savas JN, Portera-Cailliau C, Contractor A. 2018.
742 Critical period inhibition of NKCC1 rectifies synapse plasticity in the somatosensory cortex
743 and restores adult tactile response maps in fragile X mice. Mol Psychiatry. 8:109–116.
744 Heidbreder CA, Groenewegen HJ. 2003. The medial prefrontal cortex in the rat: evidence for a
745 dorso-ventral distinction based upon functional and anatomical characteristics.
746 Neuroscience & Biobehavioral Reviews. 27:555–579.
747 Hensch TK. 2016. The Power of the Infant Brain. Nature Publishing Group. 314:64–69.
748 Huguenard JR, Hamill OP, Prince DA. 1988. Developmental changes in Na+ conductances in rat
749 neocortical neurons: appearance of a slowly inactivating component. Journal of
750 Neurophysiology. 59:778–795.
751 Huttenlocher PR. 1990. Morphometric study of human cerebral cortex development.
752 Neuropsychologia. 28:517–527.
753 Kaila K, Voipio J. 1987. Postsynaptic fall in intracellular p H induced by GABA-activated
754 bicarbonate conductance. Nature. 330:163–165.
755 Khazipov R, Luhmann HJ. 2006. Early patterns of electrical activity in the developing cerebral
756 cortex of humans and rodents. Trends in Neurosciences. 29:414–418.

757 Khazipov R, Minlebaev M, Valeeva G. 2013. Early gamma oscillations. Neuroscience. 250:240–
758 252.
759 Khazipov R, Sirota A, Leinekugel X, Holmes GL, Ben-Ari Y, Buzsáki G. 2004. Early motor activity
760 drives spindle bursts in the developing somatosensory cortex. Nature. 432:758–761.
761 Kilb W. 2012. Development of the GABAergic System from Birth to Adolescence. The
762 Neuroscientist. 18:613–630.
763 Kirmse K, Kummer M, Kovalchuk Y, Witte OW, Garaschuk O, Holthoff K. 2015. GABA depolarizes
764 immature neurons and inhibits network activity in the neonatal neocortex in vivo. Nature
765 Communications. 6:7750.
766 Kolb B, Mychasiuk R, Muhammad A, Li Y, Frost DO, Gibb R. 2012. Experience and the developing
767 prefrontal cortex. Proc Natl Acad Sci USA. 109:17186–17193.
768 Konstantoudaki X, Chalkiadaki K, Tivodar S, Karagogeos D, Sidiropoulou K. 2016. Impaired
769 synaptic plasticity in the prefrontal cortex of mice with developmentally decreased number
770 of interneurons. Neuroscience. 1–13.
771 Kriegstein AR, Suppes T, Prince DA. 1987. Cellular and synaptic physiology and epileptogenesis
772 of developing rat neocortical neurons in vitro. Developmental Brain Research. 34:161–171.
773 Kroeze Y, Oti M, van Beusekom E, Cooijmans RHM, van Bokhoven H, Kolk SM, Homberg JR, Zhou
774 H. 2017. Transcriptome Analysis Identifies Multifaceted Regulatory Mechanisms Dictating a
775 Genetic Switch from Neuronal Network Establishment to Maintenance During Postnatal
776 Prefrontal Cortex Development. Cerebral Cortex. 1–19.
777 Kroon T, van Hugte E, van Linge L, Mansvelder HD, Meredith RM. 2019. Early postnatal
778 development of pyramidal neurons across layers of the mouse medial prefrontal cortex.
779 Scientific Reports. 9:5037–16.
780 Le Magueresse C, Monyer H. 2013. GABAergic Interneurons Shape the Functional Maturation of
781 the Cortex. Neuron. 77:388–405.
782 Liodis P, Denaxa M, Grigoriou M, Akufo-Addo C, Yanagawa Y, Pachnis V. 2007. Lhx6 Activity Is
783 Required for the Normal Migration and Specification of Cortical Interneuron Subtypes.
784 Journal of Neuroscience. 27:3078–3089.
785 LoTurco JJ, Owens DF, Heath MJS, Davis MBE, Kriegstein AR. 1995. GABA and glutamate
786 depolarize cortical progenitor cells and inhibit DNA synthesis. Neuron. 15:1287–1298.
787 Lu J, Karadsheh M, Delpire E. 1999. Developmental regulation of the neuronal-specific isoform
788 of K-CL cotransporter KCC2 in postnatal rat brains. J Neurobiol. 39:558–568.

789 Luhmann HJ, Prince DA. 1991. Postnatal maturation of the GABAergic system in rat neocortex.
790 Journal of Neurophysiology. 65:247–263.
791 Martina M, Royer S, Paré D. 2001. Cell-Type-Specific GABA Responses and Chloride Homeostasis
792 in the Cortex and Amygdala. Journal of Neurophysiology. 86:2887–2895.
793 McCormick DA, Prince DA. 1987. Post-natal development of electrophysiological properties of
794 rat cerebral cortical pyramidal neurones. The Journal of Physiology. 393:743–762.
795 Miyamae T, Chen K, Lewis DA, González-Burgos G. 2017. Distinct physiological maturation of
796 parvalbumin-positive neuron subtypes in mouse prefrontal cortex. J Neurosci. 3325–16–48.
797 Moore YE, Kelley MR, Brandon NJ, Deeb TZ, Moss SJ. 2017. Seizing Control of KCC2: A New
798 Therapeutic Target for Epilepsy. Trends in Neurosciences. 40:555–571.
799 Mòdol L, Bollmann Y, Tressard T, Baude A, Che A, Duan ZRS, Babij R, De Marco García NV, Cossart
800 R. 2019. Assemblies of Perisomatic GABAergic Neurons in the Developing Barrel Cortex.
801 Neuron. 1–18.
802 Owens DF, Boyce LH, Davis MBE, Kriegstein AR. 1996. Excitatory GABA Responses in Embryonic
803 and Neonatal Cortical Slices Demonstrated by Gramicidin Perforated-Patch Recordings and
804 Calcium Imaging. J Neurosci. 16:6414–6423.
805 Pan G, Yang J-M, Hu X-Y, Li X-M. 2017. Postnatal development of the electrophysiological
806 properties of somatostatin interneurons in the anterior cingulate cortex of mice. Nature
807 Publishing Group. 1–12.
808 Plotkin MD, Snyder EY, Hebert SC, Delpire E. 1997. Expression of the Na-K-2Cl cotransporter is
809 developmentally regulated in postnatal rat brains: A possible mechanism underlying GABA's
810 excitatory role in immature brain. J Neurobiol. 33:781–795.
811 Ramoa AS, McCormick DA. 1994. Developmental changes in electrophysiological properties of
812 LGNd neurons during reorganization of retinogeniculate connections. J Neurosci. 14:2089–
813 2097.
814 Rivera C, Voipio J, Payne JA, Ruusuvuori E, Lahtinen H, Lamsa K, Pirvola U, Saarma M, Kaila K.
815 1999. The K+/Cl- co-transporter KCC2 renders GABA hyperpolarizing during neuronal
816 maturation. Nature. 397:251–255.
817 Romand S, Wang Y, Toledo-Rodriguez M, Markram H. 2011. Morphological Development of
818 Thick-Tufted Layer V Pyramidal Cells in the Rat Somatosensory Cortex. Front Neuroanat. 5.
819 Rossant C, Kadir SN, Goodman DFM, et al. Spike sorting for large, dense electrode arrays. *Nat*
820 *Neurosci*. 2016;19(4):634-641. doi:10.1038/nn.4268

821 Schaeren-Wiemers N, Gerfin-Moser A. 1993. A single protocol to detect transcripts of various
822 types and expression levels in neural tissue and cultured cells: in situ hybridization using
823 digoxigenin-labelled cRNA probes. Histochemistry. 100:431–440.
824 Schubert D, Martens GJM, Kolk SM. 2014. Molecular underpinnings of prefrontal cortex
825 development in rodents provide insights into the etiology of neurodevelopmental disorders.
826 20:795–809.
827 Southwell DG, Paredes MF, Galvao RP, Jones DL, Froemke RC, Sebe JY, Alfaro-Cervello C, Tang Y,
828 García-Verdugo JM, Rubenstein JL, Baraban SC, Alvarez-Buylla A. 2012. Intrinsically
829 determined cell death of developing cortical interneurons. Nature. 491:109–113.
830 Spampanato J, Sullivan R. 2016. Development and physiology of GABAergic feedback excitation
831 in parvalbumin expressing interneurons of the mouse basolateral amygdala. Physiological
832 …. 4:e12664–15.
833 Tsujimoto S. 2008. The prefrontal cortex: functional neural development during early childhood.
834 The Neuroscientist. 14:345–358.
835 Van De Werd HJJM, Rajkowska G, Evers P, Uylings HBM. 2010. Cytoarchitectonic and
836 chemoarchitectonic characterization of the prefrontal cortical areas in the mouse. Brain
837 Struct Funct. 214:339–353.
838 Weinberger DR. 1986. Physiologic Dysfunction of Dorsolateral Prefrontal Cortex in
839 Schizophrenia. Archives of General Psychiatry. 43:114.
840 Yamada J, Okabe A, Toyoda H, Kilb W, Luhmann HJ, Fukuda A. 2004. Cl− uptake promoting
841 depolarizing GABA actions in immature rat neocortical neurones is mediated by NKCC1. The
842 Journal of Physiology. 557:829–841.
843 Yang JM, Zhang J, Yu YQ, Duan S, Li XM. 2013. Postnatal Development of 2 Microcircuits Involving
844 Fast-Spiking Interneurons in the Mouse Prefrontal Cortex. Cerebral Cortex. 24:98–109.
845 Yuan Y, Malley HAOX, Smaldino MA, Bouza AA, Hull JM, Isom LL. 2019. Delayed maturation of
846 GABAergic signaling in the Scn1a and Scn1b mouse models of Dravet Syndrome. Scientific
847 Reports. 1–16.
848 Zhang Z, Jiao Y-Y, Sun Q-Q. 2011. Developmental maturation of excitation and inhibition balance
849 in principal neurons across four layers of somatosensory cortex. Neuroscience. 174:10–25.
850 Zheng K, An JJ, Yang F, Xu W. 2011. TrkB signaling in parvalbumin-positive interneurons is critical
851 for gamma-band network synchronization in hippocampus. Proc Natl Acad Sci USA; 108
852 (41):17201-17206;

Zhu JJ. 2000. Maturation of layer 5 neocortical pyramidal neurons: amplifying salient layer 1 and layer 4 inputs by Ca2+ action potentials in adult rat tuft dendrites. The Journal of Physiology. 526:571–587.

883 **Figures and figure legends**

Figure 1

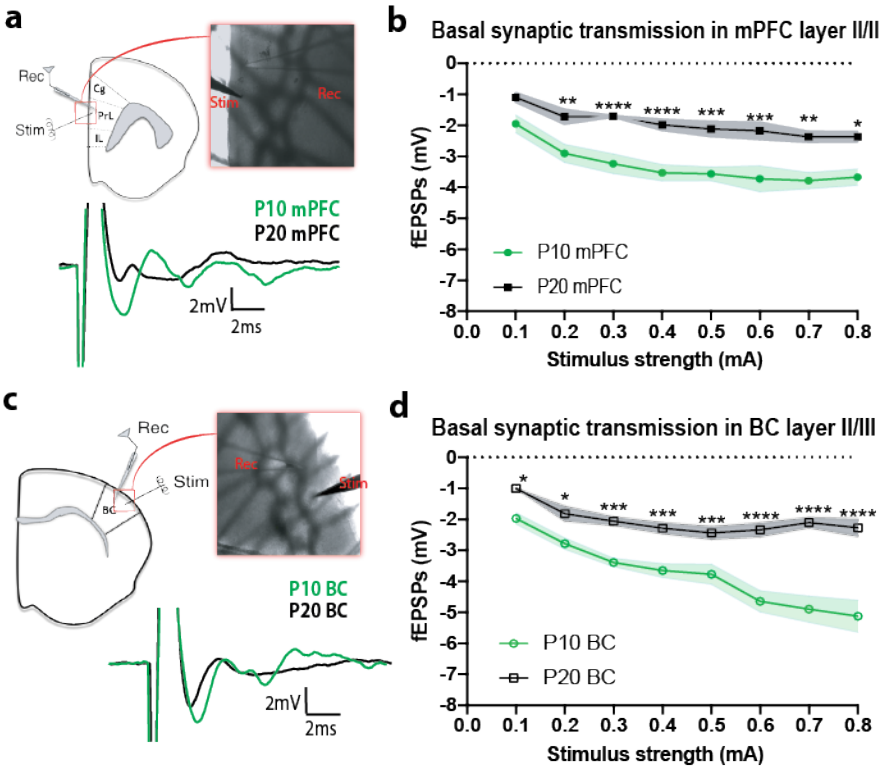

884

885 **Figure 1. Basal Synaptic transmission is decreased in mPFC and BC across development**

886 (**a, c**) (Top) Schematic representative photos showing the position of the electrodes in mPFC and
887 BC brain slices (Rec: recording electrode, Stim: stimulating electrode). (Bottom) Representative
888 traces showing the evoked field excitatory postsynaptic potentials (fEPSPs).

889 (**b,d**) Graphs showing the fEPSPs recorded in response to current pulses of increasing stimulus
890 strength in layer II/III of mPFC (**b**) and BC (**d**). Two-way repeated measures ANOVA analyses of
891 evoked fEPSPs revealed a significant effect of stimulus strength ($F_{(7, 82)} = 19.17$, $p<0.0001$) and
892 ages ($F_{(1, 82)} = 212.3$, $p<0.0001$). Post-hoc analysis showed the fEPSPs significantly decreases at
893 P20 compared to P10 in layer II/III of mPFC (Sidak's test, *p= 0.0106, **p=0.0012, ***p=0.0003
894 and ****p<0.0001) and BC (Sidak's test, *p=0.0279, ***p=0.0006 and ****p <0.0001), (n=6-7
895 brain slices from 3-4 WT male mice).

896

897

898

899

900

Figure 2

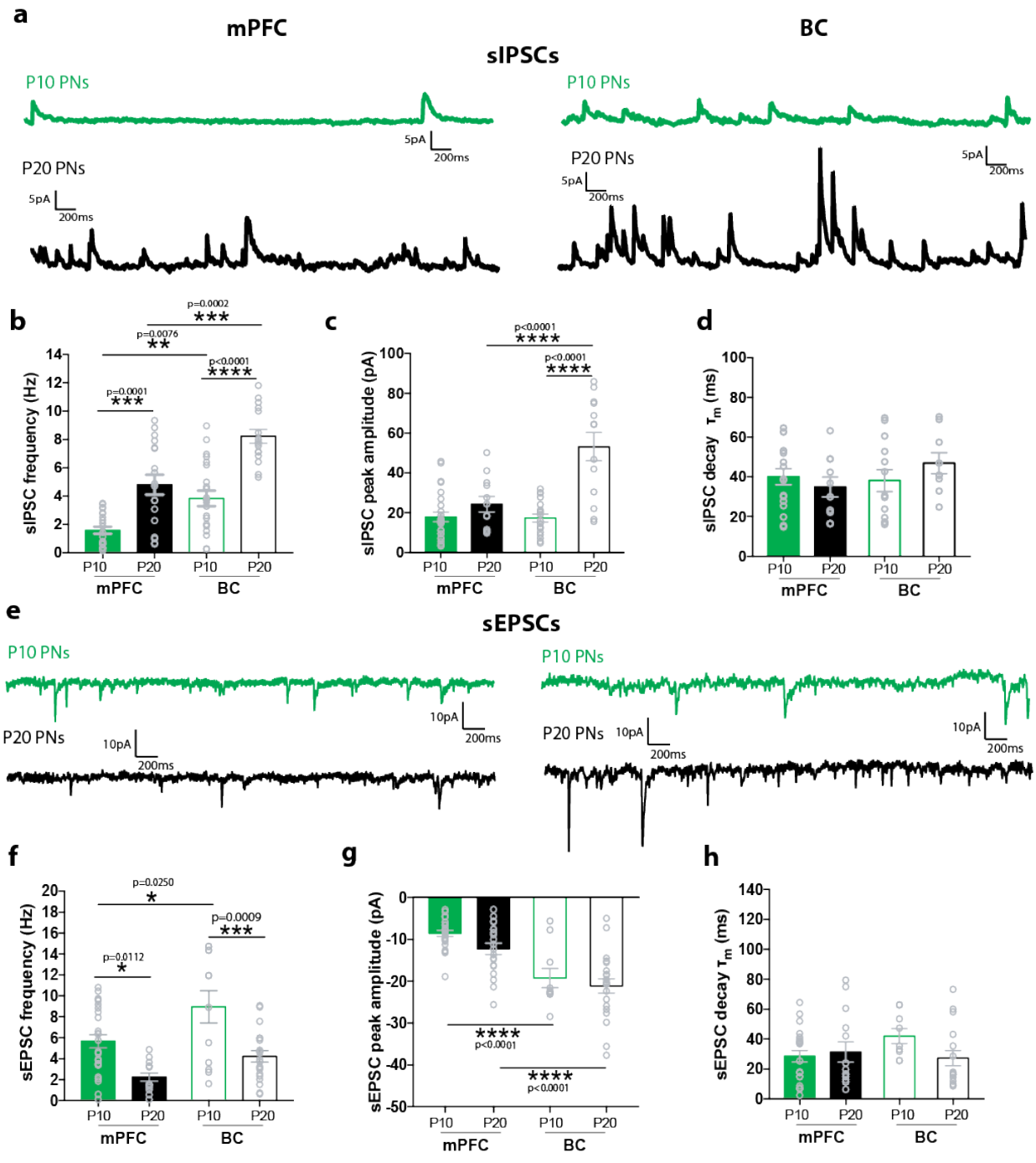

Figure 2. Properties of sIPSCs and sEPSCs at P10 and P20 of layer II/III mPFC and BC pyramidal neurons

(a) Representative traces of spontaneous inhibitory postsynaptic currents (sIPSCs) from layer II/III mPFC (left) and BC (right) pyramidal neurons at P10 (green) and P20 (black).

(b) Bar graph showing the sIPSC frequency (Hz) at P10 and P20 mPFC and BC pyramidal neurons. Two-way ANOVA analyses showed a significant effect of age ($F_{(1,74)}$=54.74, p<0.0001) and brain area ($F_{(1,74)}$=30.36, p<0.0001). Post-hoc analysis showed that sIPSC frequency was significantly

909 increased at P20 compared to P10 in mPFC (Tukey's test, p=0.0001) as well as in BC (p<0.0001).
910 Furthermore, sIPSC frequency was significantly decreased in mPFC compared to BC at P10
911 (p=0.0076) as well as at P20 (p=0.0002).
912 **(c)** Bar graph showing the sIPSC peak amplitude at P10 and P20 of mPFC and BC pyramidal
913 neurons. Two-way ANOVA analyses showed a significant effect of age ($F_{(1,65)}$=30.78, p<0.0001)
914 and brain area (($F_{(1,65)}$=13.85 p<0.0001). Post-hoc analysis showed that the sIPSC amplitude (pA)
915 was significantly increased at P20 compared to P10 in BC (p<0.0001) but not in mPFC (p=0.63).
916 The sIPSC amplitude was significantly decreased at P20 in mPFC compared to BC (p<0.0001) but
917 not at P10 between areas (p=0.9993).
918 **(d)** Bar graph showing the sIPSC decay time constant (τm) at P10 to P20 of mPFC and BC
919 pyramidal neurons. Two-way ANOVA analyses did not show any significant effect of age
920 ($F_{(1,45)}$=0.11, p=0.73) or brain area ($F_{(1, 45)}$=0.96, p=0.33) was found.
921 **(e)** Representative traces of spontaneous excitatory postsynaptic currents (sEPSCs) from layer
922 II/III mPFC (left) and BC (right) pyramidal neurons at P10 (green) and P20 (black).
923 **(f)** Bar graph showing the sEPSC frequency at P10 to P20 of mPFC and BC pyramidal neurons.
924 Two-way ANOVA analyses showed a significant effect of age ($F_{(1,68)}$=26.8, p<0.0001) and brain
925 area ($F_{(1,68)}$=10,82, p=0.0016). Post-hoc analysis showed that the sEPSCs frequency significantly
926 decreased at P20 compared to P10 in mPFC (p= 0.0112) and BC (p= 0.0009). Comparison of the
927 two brain areas at P10, the sEPSCs frequency was significantly decreased in mPFC compared to
928 BC (p= 0.0250).
929 **(g)** Bar graph showing the sEPSCs peak amplitude at P10 to P20 of mPFC and BC pyramidal
930 neurons. Two-way ANOVA analyses showed a significant effect of brain area ($F_{(1,73)}$=42.7,
931 p<0.0001) but not of age ($F_{(1,73)}$=3.435, p=0.067). The sEPSC amplitude was not significantly
932 different at P10 and P20 in mPFC (p=0.1918) and BC (p=0.8617). On the other hand, the sEPSC
933 amplitude was significantly decreased in mPFC compared to BC at P10 and P20 (p<0.0001).
934 **(h)** Bar graph showing the sEPSCs decay time constant (τm) at P10 to P20 of mPFC and BC
935 pyramidal neurons. Two-way ANOVA analyses showed no significant effect of age ($F_{(1,57)}$=0.22,
936 p=0.27) or brain area ($F_{(1,57)}$=0.77, p=0.39).
937 *All post-hoc tests values were based on Tukey's test; n=9-13 cells from 5-9 mice/age group.
938
939

Figure 3

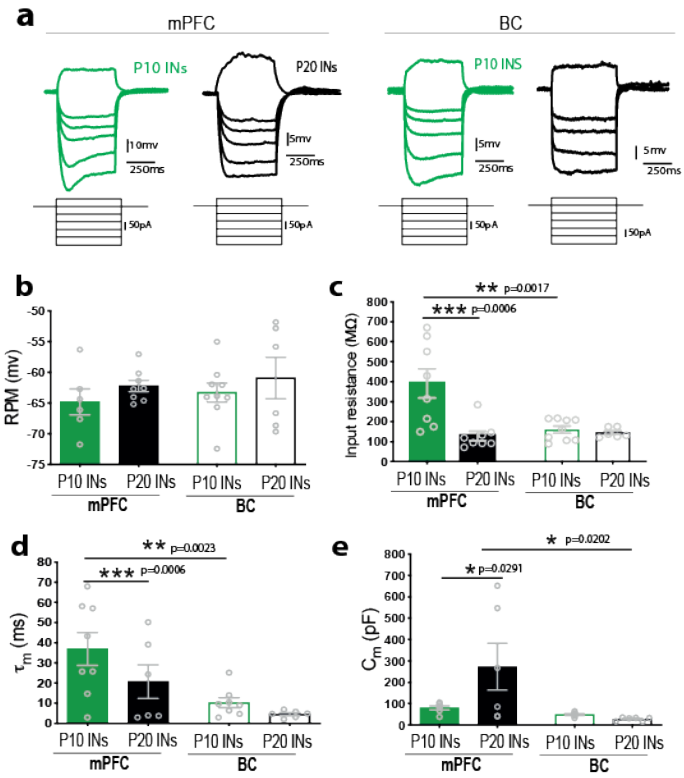

Figure 3. Passive membrane properties of Lhx6+ interneurons at P10 and P20 mPFC and P10 BC.

(a) Representative voltage responses (top traces) to 500ms positive and negative current pulses (bottom traces, +50, -50, -70, -100, -150, -200 pA) in mPFC at P10 and P20 and BC of Lhx6+ florescent interneurons from layer II/III.

(b) Bar graph showing the resting membrane potential (RMP) of interneurons at P10 and P20 in mPFC and BC. Two-way ANOVA analyses did not show any significant effect of age ($F_{(1,25)}$=1.55, p=0.22) or brain area ($F_{(1, 25)}$=0.50, p=0.48) was found., (n=6-9 cells from 5-6 mice/age group).

(c) Bar graph showing the input resistance of interneurons at P10 and P20 in mPFC and BC. Two-way ANOVA analyses showed a significant effect of age ($F_{(1,27)}$=10.94, p=0.0027) and brain area ($F_{(1,27)}$=6.65 p=0.0157). Post-hoc analysis showed that the input resistance significantly decreased at P20 compared to P10 in mPFC (Tukey's test, p=0.0006) and was significantly higher in mPFC compared with BC, at P10 (Tukey's test, p=0.0017), (n=8-9 cells from 5-6 mice/age group).

(d) Bar graph showing the membrane time constant (τ_m) of interneurons at P10 and P20 in mPFC and BC. Two-way ANOVA analyses showed a significant effect of age ($F_{(1,24)}$=14.71, p=0.0008) and brain area ($F_{(1,24)}$=6.92 p=0.0147). Post-hoc analysis showed that τ_m was

958 significantly higher at P10 compared to P20 in mPFC (Tukey's test, p=0.0006) while it was
959 significantly higher in mPFC compared to BC, at P10 (Tukey's test, p=0.0023), (n=8-9 cells from
960 5-6 mice/age group).
961 **(e)** Bar graph showing the membrane capacitance (C_m) of interneurons at P10 and P20 in mPFC
962 and BC. Two-way ANOVA analyses showed a significant effect between brain areas ($F_{(1,21)}$=6.82,
963 p=0.00163) and not between ages ($F_{(1,21)}$=2.60 p=0.1219). Post-hoc analysis showed that Cm was
964 significantly higher at P10 compared with P20 in mPFC (Tukey's test, p=0.0291) and was not
965 significantly different between mPFC and BC, at P10 (Tukey test, p=0.97) while it was significantly
966 higher at P20 in mPFC compared to P20 in BC (Tukey test, p=0.0202), (n=6-9 cells from 5-6
967 mice/age group).
968
969
970
971
972
973
974
975
976
977
978
979
980
981
982
983
984
985
986
987
988
989

Figure 4

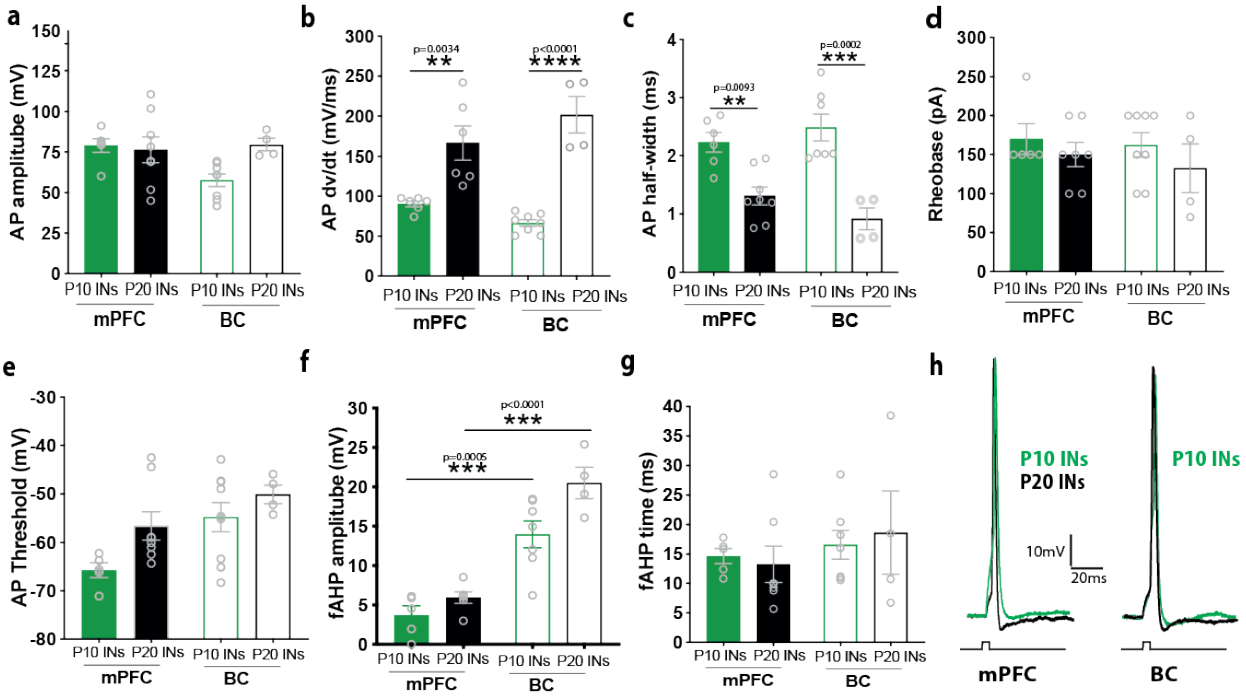

Figure 4. Poor development of active membrane properties of Lhx6⁺ interneurons in mPFC.

(a) Bar graph showing the action potential (AP) amplitude of interneurons at P10 and P20 in mPFC and BC. Two-way ANOVA analyses did not show any significant effect of age ($F_{(1,22)}$=2.46, p=0.13) or brain area ($F_{(1, 22)}$=2.13, p=0.15) was found., (n=6-9 cells from 5-6 mice/age group).

(b) Bar graph showing the AP rate of rise (dv/dt) of interneurons at P10 and P20 in mPFC and at P10 in BC. Two-way ANOVA analyses showed a significant effect between ages ($F_{(1,20)}$=58.96, p<0.0001) but not brain area ($F_{(1,20)}$=0.16 p=0.69). Post-hoc analysis showed that the AP rate of rise significantly increased at P20 compared to P10 in mPFC (Tukey's test, p=0.0034) and at P20 compared to P10 in BC (Tukey's test, p<0.001), (n=6-9 cells from 5-6 mice/age group).

(c) Bar graph showing the AP duration (half-width) of interneurons at P10 and P20 in mPFC and BC. Two-way ANOVA analyses showed a significant effect between ages ($F_{(1,21)}$=39.16, p<0.0001) but not brain area ($F_{(1,21)}$=0.16 p=0.73). Post-hoc analysis showed that the AP duration significantly decreased at P20 compared to P10 in mPFC (Tukey's test, p= 0.0093) and at P20 compared to P10 in BC (Tukey's test, p=0.0002), (n=6-9 cells from 5-6 mice/age group).

(d) Bar graph showing the AP rheobase of interneurons at P10 and P20 in mPFC and BC. Two-way ANOVA analyses did not show any significant effect of age ($F_{(1,20)}$=1.60, p=0.22) or brain area ($F_{(1, 20)}$=0.40, p=0.53) was found.

1009 **(e)** Bar graph showing the AP threshold of interneurons at P10 and P20 in mPFC and BC. . Two-
1010 way ANOVA analyses showed significant effect of age ($F_{(1,22)}$=5.048, p=0.035) and brain area ($F_{(1,}$
1011 $_{22)}$=8.00, p=0.009) was found. Post-hoc analysis showed that the AP threshold was not
1012 significantly different at P20 compared to P10 in mPFC (Tukey's test, p=0.1673) and in BC
1013 (Tukey's test, p=0.72009) or at P10 in mPFC compared to P10 in BC (Tukey's test, p=0.067) and
1014 at P20 in mPFC compared to P20 in BC (Tukey's test, p=0.72).
1015 **(f)** Bar graph showing the AHP (afterhypolarization) amplitude of interneurons at P10 and P20
1016 in mPFC and BC. Two-way ANOVA analyses showed significant effect of age ($F_{(1,18)}$=7.35,
1017 p=0.0143) and brain area ($F_{(1, 18)}$=63.72, p<0.0001) was found. Post-hoc analysis showed that the
1018 AHP amplitude was not significantly different at P20 compared to P10 in mPFC (Tukey's test,
1019 p=0.7187) and was significantly decreased in mPFC compered to BC, at P10 (Tukey's test, p=
1020 0.0005) and in mPFC compered to BC at P20 (Tukey's test, p<0.00001), (n=6-9 cells from 5-6
1021 mice/age group).
1022 **(g)** Bar graph showing the AHP time of interneurons at P10 and P20 in mPFC and BC. Two-way
1023 ANOVA analyses did not show any significant effect of age ($F_{(1,19)}$=0.009, p=0.92) or brain area
1024 ($F_{(1, 19)}$=1.074, p=0.31) was found.
1025 **(h)** Representative traces of APs of layer II/III Lhx6+ interneurons in mPFC (left) and BC (right)
1026 at P10 (green) and P20 (black).
1027
1028
1029
1030
1031
1032
1033
1034
1035
1036
1037
1038
1039
1040

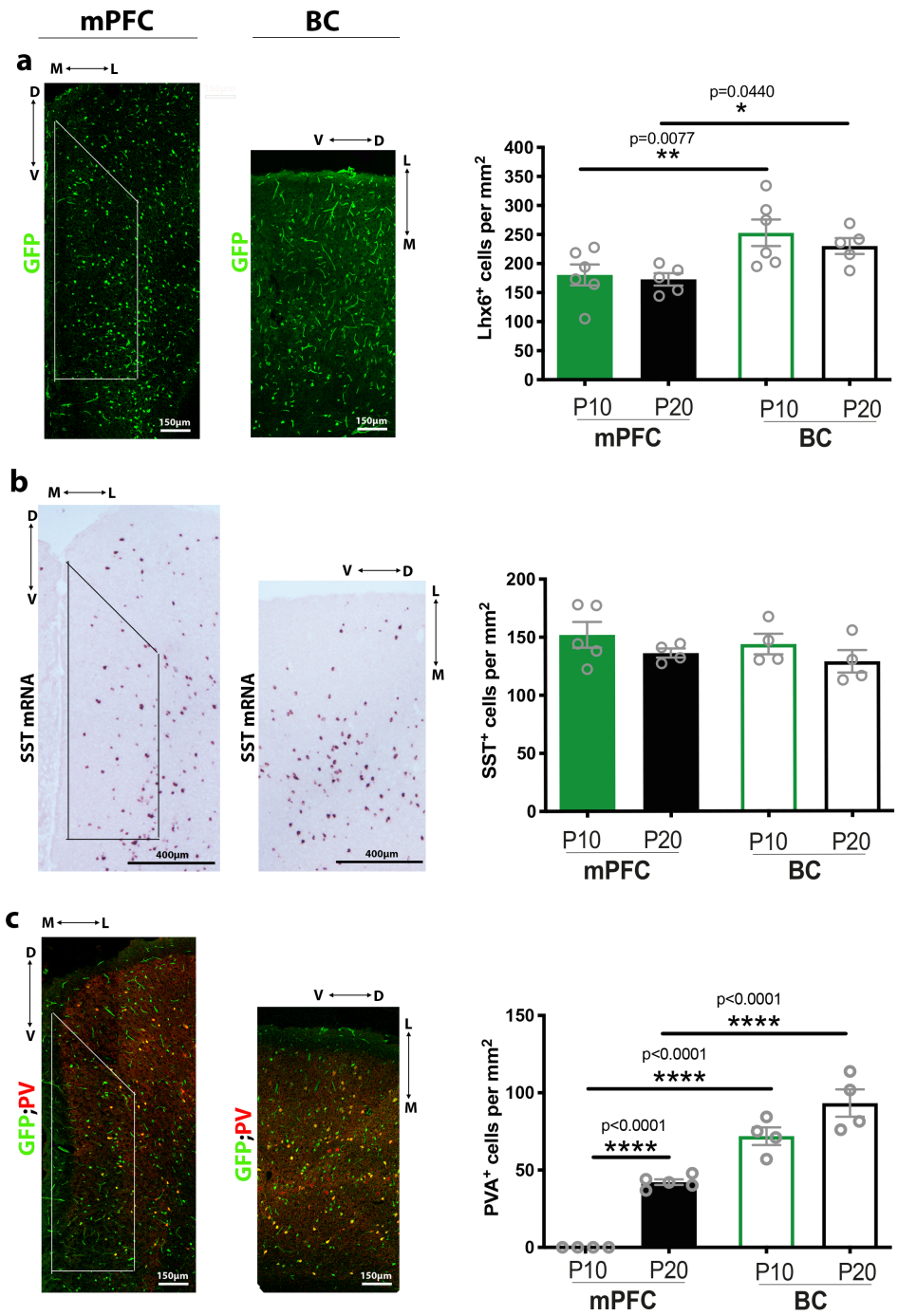

Figure 5. Significant differences in cellular density of Lhx6⁺ interneurons in mPFC and BC at P10 and P20.

(a) A representative immunostaining with GFP for Lhx6⁺ interneurons in Lhx6-cre;ROSA26fl-STOPfl-YFP mice in mPFC and BC at P20 is showing on the left. Scale bars: 150 µm. On the right, bar graph comparing Lhx6⁺ interneurons cell density (per mm^2) at P10 and P20 in mPFC and BC. Two-way ANOVA analyses of the cell density revealed a significant effect of brain area ($F_{(1, 18)}$ =

1049 13.11, p=0.0020), but not of age ($F_{(1,18)}$=0.7185, p=0.4078). Post-hoc analysis showed that the
1050 Lhx6$^+$ cell density was not significant different at P20 compared to P10 in mPFC and BC (LSD test,
1051 p=0.77 and p= 0.38, respectively). The Lhx6$^+$ cell density was significantly lower in mPFC
1052 compared to BC at P10 and P20, respectively (LSD test, p=0.0077 and p= 0.0440, respectively),
1053 (P10 in mPFC and BC:n= 5 mice, P20 in mPFC and BC: n=4).
1054 **(b)** A representative in situ hybridization staining for somatostatin positive cells (SST$^+$) using
1055 wild type animals in mPFC and BC at P20 is showing on the left. Scale bar: 200µm. Bar graph
1056 comparing cell density based on SST$^+$ expression at P10 and P20 in mPFC and BC. Two-way
1057 ANOVA analyses of the cell density showed no significant effect of age ($F_{(1, 13)}$= 2.78, p=0.12) and
1058 brain area ($F_{(1,13)}$=071, p=0.41) was found, (P10 in mPFC: n= 5 mice, P10 in BC and P20 in mPFC
1059 and BC: n=4).
1060 **(c)** A representative double immunostaining for GFP; PV (PV: parvalbumin) in mPFC and BC at
1061 P20 is showing on the left. Scale bars: 150 µm. On the right, bar graph comparing cell density
1062 based on PV$^+$ expression at P10 and P20 in mPFC and BC. Two-way ANOVA analyses of the cell
1063 density revealed a significant effect of age ($F_{(1, 14)}$ = 45.49, p<0.0001) and brain area ($F_{(1, 14)}$ =
1064 170.2, p<0.0001). PV$^+$ cells were not found in mPFC but were identified in BC, at P10. Post-hoc
1065 analysis showed that the PV$^+$ cell density was not significantly different at P20 compared to P10
1066 in BC (LSD test, p= 0.1089), but was significantly lower in mPFC compared to BC at P20 (LSD test,
1067 p<0.0001), (P10 and P20 in mPFC: n= 5 mice, P10 and P20 in BC: n=4).
1068
1069
1070
1071
1072
1073
1074
1075
1076
1077
1078
1079
1080

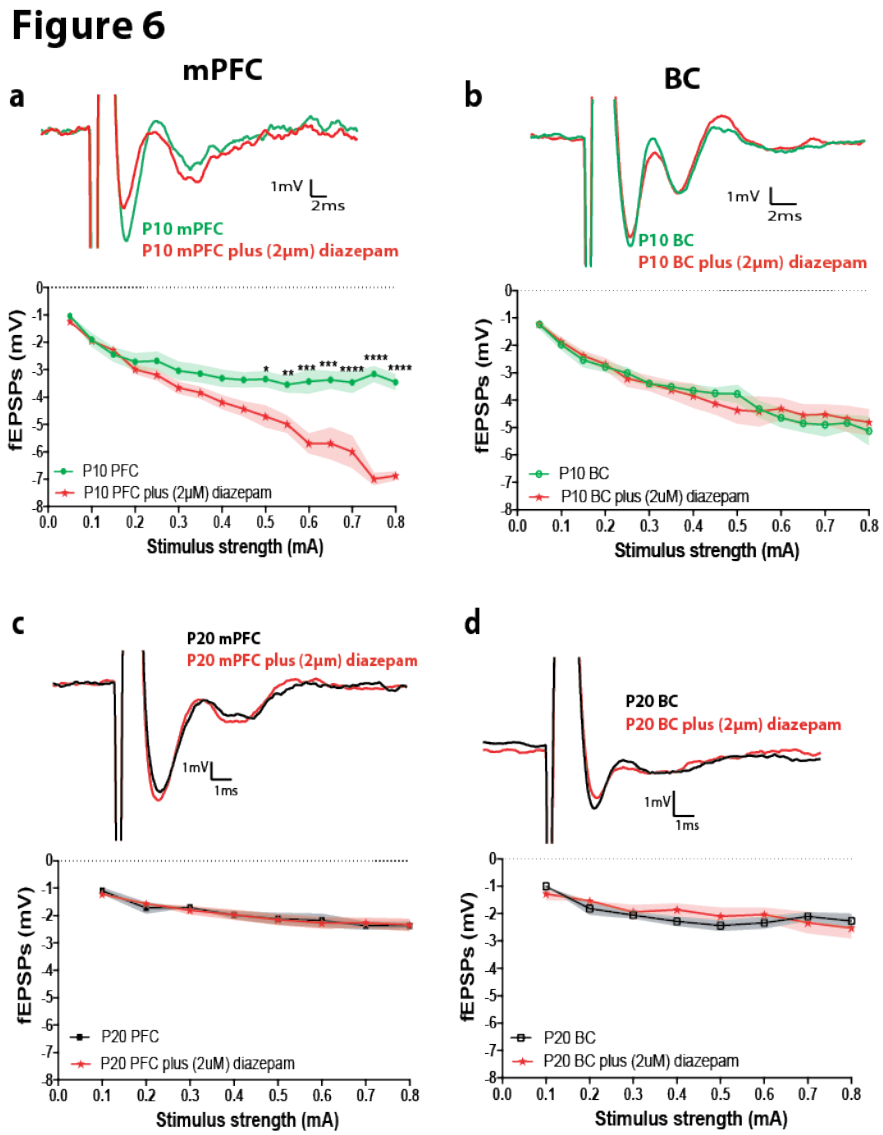

Figure 6. Increased $GABA_AR$ activity leads to enhanced fEPSPs in mPFC during the second postnatal week.

fEPSPs were recorded were recorded in layer II/III in response to current pulses of increasing stimulus strength of layer II/III, during two experimental treatments, before and after application of 2µM diazepam ($GABA_AR$ agonist) at P10 and P20 of mPFC and BC in mice.

(a) Representative traces (left) and graph (right) showing the fEPSPs amplitude before (green) and after (red) diazepam bath application, in mPFC at P10. Two-way repeated measures ANOVA analyses of evoked fEPSPs revealed significant effect of stimulus strength ($F_{(15,135)}$ = 25.64, p<0.0001) and experimental treatments ($F_{(1, 135)}$ = 136.1, p<0.0001). Post-hoc analysis showed that the fEPSP amplitude significantly increased in mPFC at P10 after diazepam bath application

1093 (Sidak's test, *p= 0.0175, **p=0.0082, ***p=0.0002 and ****p<0.0001 at 0.3, 0.4. 0.5, 0.6 and
1094 0.7 mA respectively), (n=6-7 brain slices from 3-4 mice).
1095 **(b)** Graph (right) and representative traces (left) showing that diazepam bath application does
1096 not have any effect on the fEPSP amplitude in BC at P10. Two-way repeated measures ANOVA
1097 analyses of evoked fEPSPs revealed a significant effect of stimulus strength (F (15, 140) = 24.05,
1098 p<0.0001) but not experimental conditions ($F_{(1, 135)}$ = 0.03, p=0.86), (n=6-7 brain slices from 3-4
1099 mice).
1100 **(c)** Graph (right) and representative traces (left) showing that diazepam bath application does
1101 not have any effect on the fEPSP amplitude in mPFC at P20. Two-way repeated measures ANOVA
1102 analyses of evoked fEPSPs revealed a significant effect of stimulus strength ($F_{(7, 96)}$ = 10.36,
1103 p<0.0001) but not experimental conditions ($F_{(1,96)}$=0.03, p=0.9382), (n=6-7 brain slices from 3-4
1104 mice).
1105 **(d)** Graph (right) and representative traces (left) showing that bath application of diazepam
1106 does not have any effect in the fEPSP amplitude in BC at P20. Two-way repeated measures
1107 ANOVA analyses of evoked fEPSPs revealed a significant effect of stimulus strength ($F_{(7, 96)}$ = 5.51,
1108 p<0.0001) but not experimental conditions ($F_{(1, 96)}$ = 0.50, p=0.47), (n=6-7 brain slices from 3-4
1109 mice).
1110
1111
1112
1113
1114
1115
1116
1117
1118
1119
1120
1121
1122
1123
1124

Figure 7

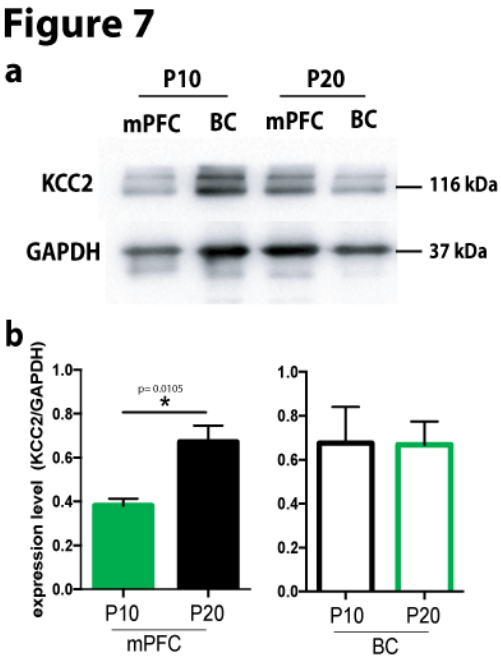

Figure 7. Decreased levels of K+-Cl- co-transporter 2 (KCC2) in mPFC during the second postnatal week.

(a) Representative blots showing changes of the K-Cl co-transporter (KCC2) levels, relative to GAPDH at P10 and P20 in mPFC and BC.

(b) Graph showing the normalized protein level (KCC2/GAPDH) in mPFC and BC at P10 and P20. The KCC2 protein levels was significantly increased at P20 compared to P10 in mPFC (two-tailed t-test, p= 0.01) but not in BC (two-tailed t-test, p= 0.97) (n=3-4 mice).

Figure 8

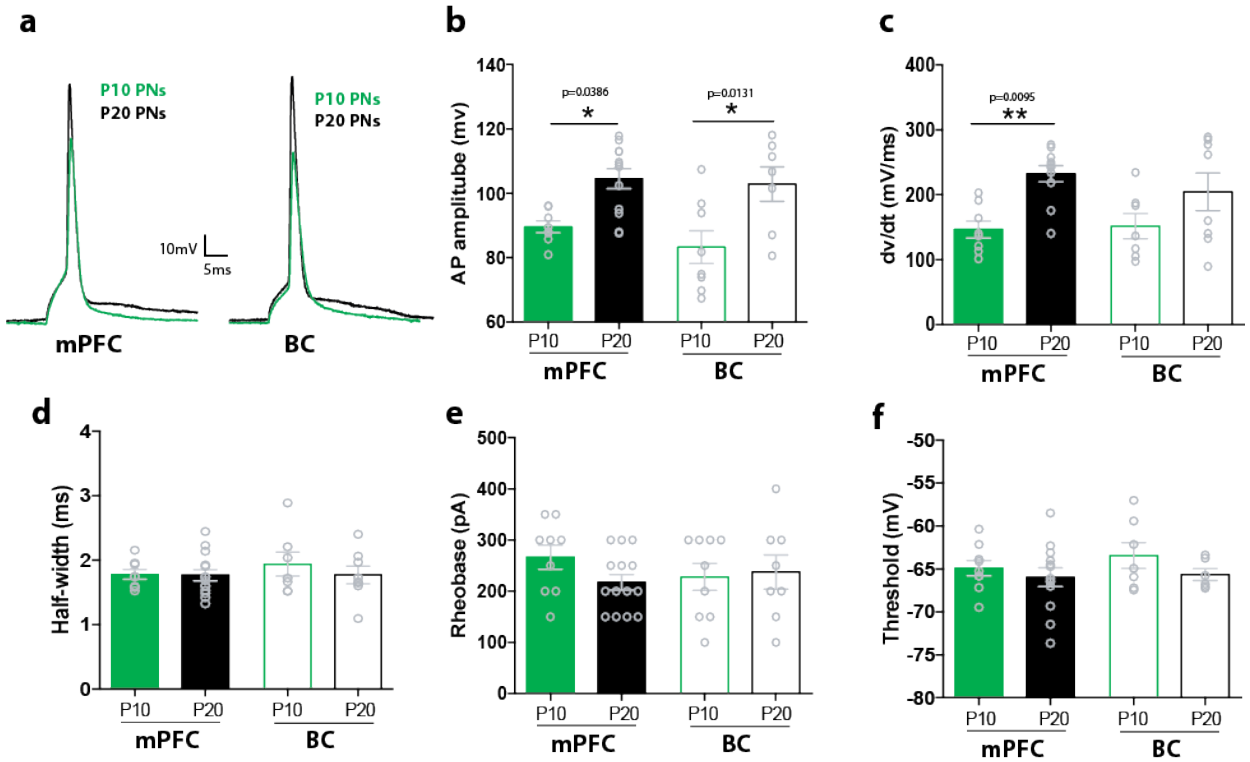

Figure 8. Active properties of mPFC and BC pyramidal neurons.

(a) Representative traces of action potentials (APs) of layer II/III pyramidal neurons in mPFC (left) and BC (right) at P10 (green) and P20 (black), respectively.

(b) Bar graph showing the AP amplitude of pyramidal neurons at P10 and P20 in mPFC and BC. Two-way ANOVA analyses showed a significant effect of age ($F_{(1, 31)}$ = 18.74, p=0.0001) but not on brain area ($F_{(1, 31)}$ = 0.99, p=0.32) was found. Post-hoc analysis showed that the AP amplitude significantly increased at P20 compared to P10 in mPFC and BC (Tukey's test, p=0.0386 and p= 0.0131, respectively) (n=9-14 cells from 6-10 mice/age group).

(c) Bar graph showing the AP rate of rise (dv/dt) of pyramidal neuron at P10 and P20 in mPFC and BC. Two-way ANOVA analyses showed a significant effect of age ($F_{(1,30)}$= 13.53, p=0.0009) but not on brain area ($F_{(1, 30)}$ = 0.36, p=0.55) was found. Post-hoc analysis showed that the AP rate of rise significantly increased at P20 compared to P10 in mPFC (Tukey's test, p= 0.0095), but not in BC (Tukey's test, p= 0.25) (n=8-14 cells from 6-10 mice/age group).

(d) Bar graph showing the AP duration (half-width) of pyramidal neuron at P10 and P20 in mPFC and BC. Two-way ANOVA analyses showed no significant effect of age (F(1, 33) = 0.52, p=0.47) or brain area ($F_{(1, 33)}$ = 0.43, p=0.51) was found (n=9-14 cells from 6-10 mice/age group).

1162 **(e)** Bar graph showing the AP rheobase of pyramidal neuron at P10 and P20 in mPFC and BC.
1163 Two-way ANOVA analyses showed no significant effect of age ($F_{(1, 36)} = 0.66$, $p=0.41$) or brain
1164 area ($F_{(1, 36)} = 0.16$, $p=0.69$) was found (n=9-14 cells from 6-10 mice/age group).
1165 **(f)** Bar graph showing the AP threshold of pyramidal neuron at P10 and P20 in mPFC and BC.
1166 Two-way ANOVA analyses showed no significant effect of age ($F_{(1,31)} = 1.90$, $p=0.17$) or brain area
1167 ($F_{(1,31)}=0.55$, $p=0.46$) was found (n=9-14 cells from 6-10 mice/age group).
1168
1169
1170
1171
1172
1173
1174
1175
1176
1177
1178
1179
1180
1181
1182
1183
1184
1185
1186
1187
1188
1189
1190
1191
1192
1193

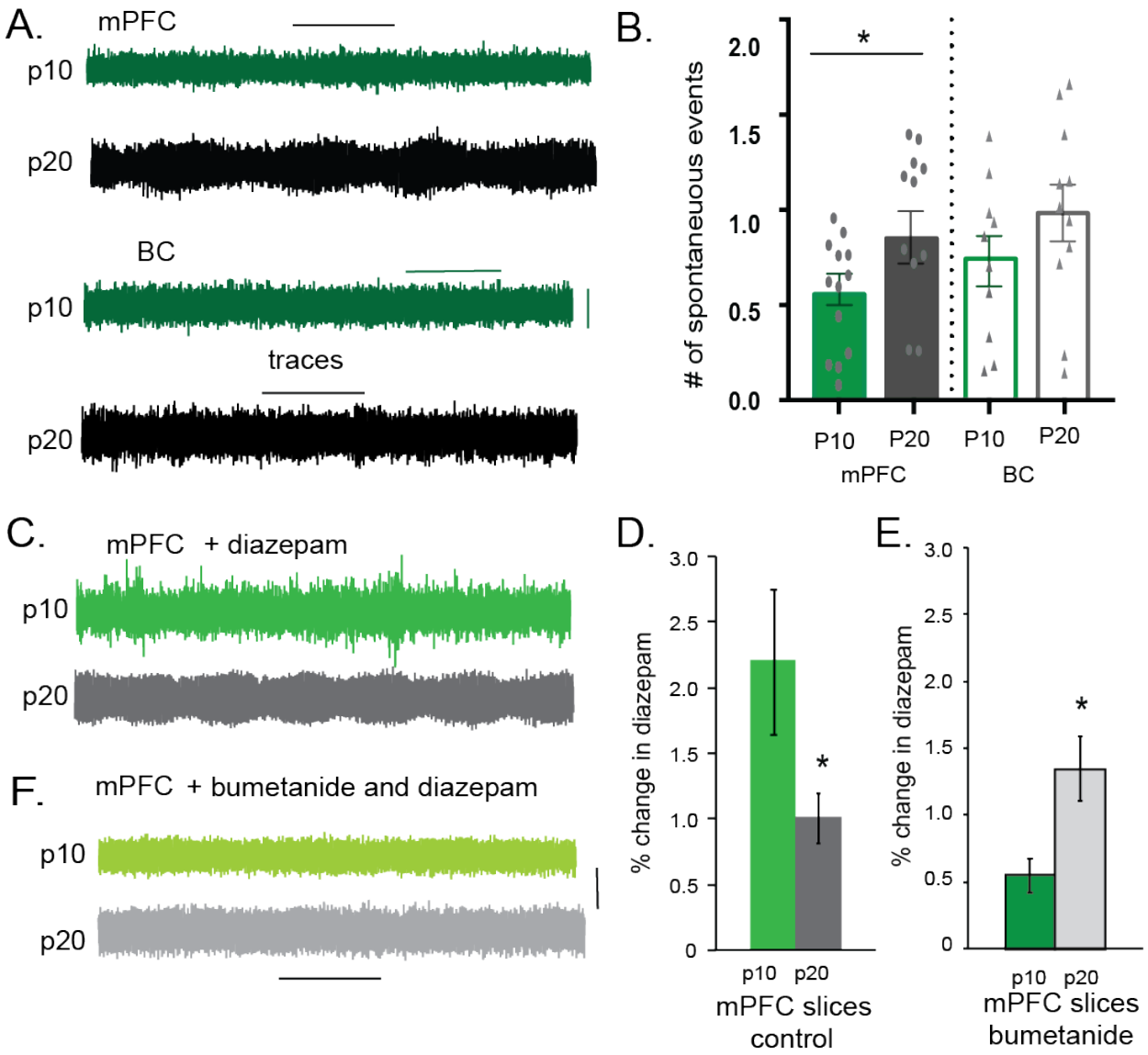

Figure 9. Spontaneous activity events in mPFC and BC brain slices.

(a) Representative traces of spontaneous activity in mPFC and BC brain slices at P10 and P20.

(b) Graph showing that the number of spontaneous activity events in mPFC and BC brain slices at P10 and P20. Two-way ANOVA analyses showed a significant effect of age ($F_{(1,32)}$= 11.48, p=0.0016) but not on brain area ($F_{(1, 39)}$ = 0.09, p=0.77) was found. The number of spontaneous events was significantly increased in the mPFC at P20 compared to P10 (Sidak's test, p= 0.0132), but in BC at P20 compared to P10 (Sidak's test, p= 0.5851).

(c) Representative traces of spontaneous activity in mPFC following the addition of diazepam and diazepam + bumetanide at P10 and P20.

(d) Graph showing that the percent change due to diazepam is significantly increased at P10, compared to P20 (t-test, p=0.02).

(e) Graph showing that the percent change due to diazepam, in the presence of bumetanide, is significantly reduced at P10, compared to P20 (t-test, p=0.03).

1238 **Figure 10**

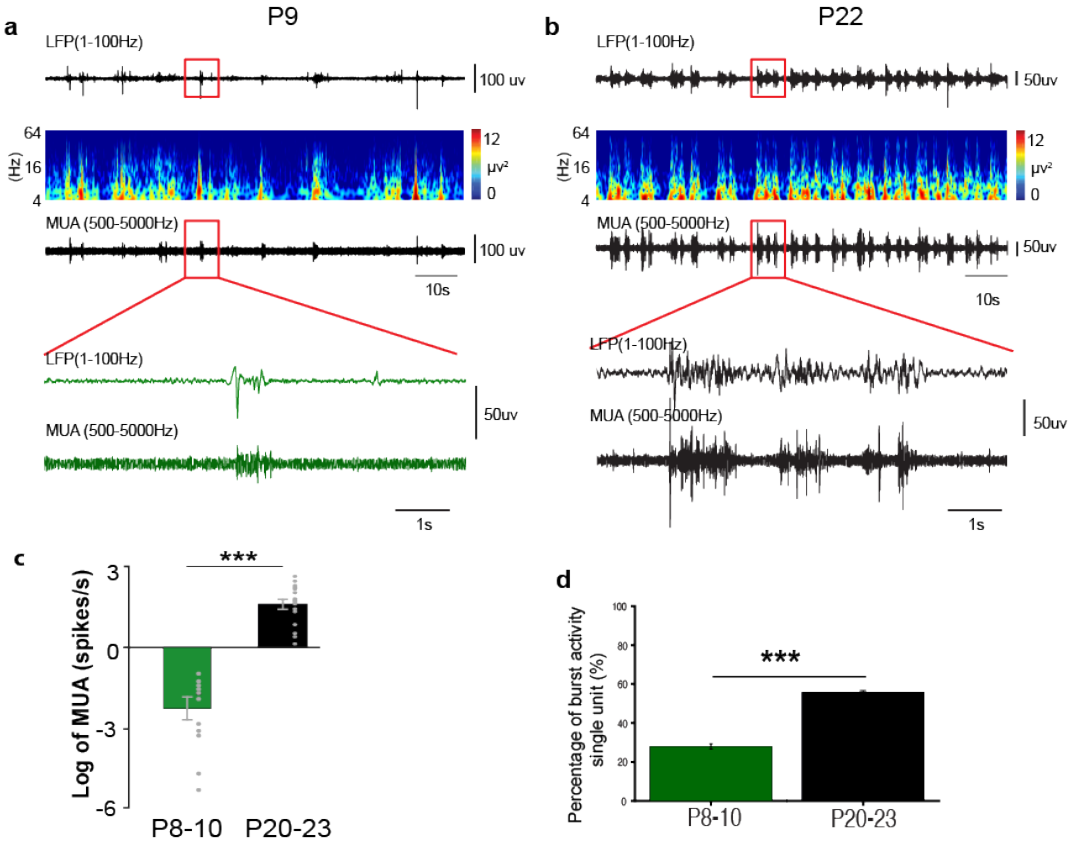

1239

1240

1241 **Figure 10. Spike activity in PFC of neonatal and pre-juvenile mice.**

1242 **(a)** Extracellular LFP recordings of oscillatory activity in PFC from a P9 mouse displayed after
1243 bandpass (1-100 Hz) filtering (top) and the corresponding MUA after bandpass (500-5000 Hz)
1244 filtering (bottom). Traces are accompanied by the color-coded wavelet spectra of the LFP at
1245 identical time scale.

1246 **(b)** the same display as (**a**), but in one P22 mouse.

1247 **(c)** Bar diagram displaying the mean MUA of neurons in PFC of neonatal and pre-juvenile mice.
1248 During development, significant increase of MUA in PFC in pre-juvenile mice (n=14) compared
1249 with in neonatal mice (n=13) (1.71±0.16 vs. -2.29±0.45, $p<0.0001$, One-way ANOVA, $F_{(1,}$
1250 $_{25)}$=80.19).

1251 **(d)** Bar diagram displaying the percentage of the burst activity of single units in PFC of neonatal
1252 and pre-juvenile mice. During development, significant more burst activity per single unit in PFC
1253 in pre-juvenile mice (150 single unit) than in neonatal mice (161 single unit) (55.73±0.92 % vs.
1254 27.90±1.41 %, $p<0.0001$, One-way ANOVA, F(1, 309)=272.26). In neonatal mice, 21 out 161 single

1255 units were classified as “burst unit”. In pre-juvenile mice, 104 out of 150 single units were
1256 classified as “burst unit”.
1257